ANALYSIS OF BIOMEDICAL SIGNALS PROCESSING TECHNIQUES

A THESIS

SUBMITTED TO THE DELHI TECHNOLOGICAL UNIVERSITY

FOR THE AWARD OF THE DEGREE OF

DOCTOR OF PHILOSOPHY

IN

ELECTRONICS & COMMUNICATION ENGINEERING

SUBMITTED BY

MAHIPAL SINGH CHOUDHRY

DEPARTMENT OF ELECTRONICS & COMMUNICATION ENGINEERING

DELHI TECHNOLOGICAL UNIVERSITY

(Formerly Delhi College of Engineering)

DELHI- 110042 (INDIA)

NOVEMBER -2016

ANALYSIS OF BIOMEDICAL SIGNALS PROCESSING TECHNIQUES

A THESIS

SUBMITTED TO THE DELHI TECHNOLOGICAL UNIVERSITY

FOR THE AWARD OF THE DEGREE OF

DOCTOR OF PHILOSOPHY

IN

ELECTRONICS & COMMUNICATION ENGINEERING

SUBMITTED BY

MAHIPAL SINGH CHOUDHRY

DEPARTMENT OF ELECTRONICS & COMMUNICATION ENGINEERING

DELHI TECHNOLOGICAL UNIVERSITY

(Formerly Delhi College of Engineering)

DELHI- 110042 (INDIA)

NOVEMBER -2016

CERTIFICATE

This is to certify that the thesis entitled "**Analysis of Biomedical Signals Processing Techniques**" being submitted by Mr**. Mahipal Singh Choudhry (**Reg No: 2K11/PHD/EC/10) for the award of the degree of Doctor of Philosophy to the Delhi Technological University is based on the original work carried out by him. He has worked under my supervision and has fulfilled the requirements, which to my knowledge have reached the requisite standard for the submission of this thesis. It is further certified that the work embodied in this thesis has neither partially not fully submitted to any other university nor institution for the award of any degree or diploma.

Prof. Rajiv Kapoor
(Supervisor)
Department of Electronics & Communication Engineering
Delhi Technological University, Delhi.

ACKNOWLEDGMENTS

I'm in debt and would like to express a great feeling of gratitude towards several people who guided and supported me throughout the completion of my research program.

First and foremost, I would like to thank my supervisor, **Prof. Rajiv Kapoor**, for his support and faith in me during the course of my Ph.D. studies. My research work cannot be turned into a prodigious experience without his substantial and thorough approach, together with his unpretentious interest in the research subject.

Above all, my deepest thanks go to my parents and brother for their absolute affection and support. Also, my wholehearted recognition to my wife (**Kiran**), my daughter (**Anushka**) and my son (**Aditya**) for their love, affection, patience and everyday devotion that made it possible to complete this research work.

Finally, but not lastly, I would also like to express my sincere thanks to all those who supported me directly and indirectly along with my colleagues (especially **Dr. D. K. Vishwakarma**) for their encouragement and advice, which they provided me during this research journey.

Date: (Mahipal Singh Choudhry)

Place: Delhi

ABSTRACT

The biomedical signal is a summarizing term for all kinds of signals that can be continually measured and monitored from biological beings. Electrocardiogram (ECG) and Electroencephalogram (EEG) are most important 1-D biomedical signals as they are linked with activities of heart and brain respectively, the most important organs of human body.

Magnetic Resonance Imaging (MRI) is the most popular medical imaging technique. It has a wide range of applications in medical diagnosis and it is preferred over other methods for medical imaging purpose for the reason that it does not involve any ionizing radiation. Importance of MRI can be understood with the fact that over 50,000 MRI scanners are estimated to be in use worldwide for biomedical imaging purpose.

Acquisition of a biomedical signal is not sufficient but it is required to process the acquired signal to get the relevant information “buried” in it. This may be due to the fact that the signal is affected by noise during signal acquisition and thus must be “cleaned” using some signal processing technique or method to minimize effects of noise and to enhance useful information. There are different types of noises or artifacts in biomedical signals. Baseline wander and ocular artifacts are the most important artifacts in case of ECG and EEG respectively.

This research is mainly focused on proposing novel methods for removal of baseline wander and ocular artifact from ECG and EEG. A new method is proposed for baseline wander artifact denoising from ECG using a cascaded combination of Complete Ensemble Empirical Mode Decomposition (CEEMD) and Morphological functions with adaptive Structure Elements (SEs). The proposed method maintains morphology of ECG during denoising and denoising performance is independent of heart rate in case of stress ECG.

A new method is proposed for ocular artifact removal from EEG using Stationary Wavelet Enhanced Independent Component Analysis (ICA) with a novel threshold technique. The proposed method preserves morphological information present in EEG and the novel threshold technique makes denoising more efficient.

MR image is the most important 2-D biomedical signal (Biomedical Image) and segmentation is one of the most important steps of MRI denoising and classification. A novel fuzzy energy based level set method is proposed in this research work for segmentation of MR images. Proposed method deals effectively and simultaneously with intensity inhomogeneity and noise problems of medical image by integrating active contour with Fuzzy C-Means (FCM) clustering. Denoising of MR images is further enhanced by using a mean filter based spatial term with proposed FCM based energy function.

Performance of proposed methods is tested with various publicly available datasets and compared with earlier state-of-the-art methods.

LIST OF PUBLICATIONS

Mahipal Singh Choudhry, Rajiv Kapoor "*Performance Analysis of Fuzzy C-Means Clustering Methods for MRI Image Segmentation*", Procedia Computer Science Journal (Pub: Elsevier), 2016, vol .89, pp: 749-756.

Mahipal Singh Choudhry, Rajiv Kapoor "*A Novel Fuzzy Energy Based Level Set Method for Medical Image Segmentation*", Cogent Engineering, 5:1475032 (Pub: Cogent OA, Taylor & Francis), 2018.

Mahipal Singh Choudhry, Rajiv Kapoor "*Ocular Artifact Removal from EEG using Stationary Wavelet Enhanced ICA*", International Journal of Control Theory and Applications (ISSN: 0974-5572, Scopus Indexed Journal with SJR: 0.53), 2016, vol: 9, no: 10, pp: 4935-4945.

Mahipal Singh Choudhry, Rajiv Kapoor "*Removal of Baseline Wander from ECG using CEEMD and Adaptive Morphological Functions*", Journal of Chemical and Pharmaceutical Science (ISSN: 0974-2115, Scopus Indexed Journal with SJR: 0.12), No. 04, pp. 31–37, October 2016.

Mahipal Singh Choudhry at el., "*Removal of Baseline Wander from ECG signal using Empirical Mode Decomposition and Morphological Functions*", IEEE 3rd International Conference on Signal Processing and Integrated Networks (SPIN-2016), 11 Feb-12 Feb 2016, Amity University, Noida, India.

Mahipal Singh Choudhry at el., "*A Survey on Different Discrete Wavelet Transforms and Thresholding Techniques for EEG Denoising*" IEEE International Conference on Computing Communication and Automation (ICCCA 2016), 29-30 April 2016, Galgotias University, Greater Noida, India.

Mahipal Singh Choudhry at el., "*Comparison between Different Wavelet Transforms and Thresholding Techniques for ECG Denoising*", IEEE International Conference on Advances in Engineering & Technology Research (ICAETR - 2014), August 01-02, 2014, Dr. Virendra Swarup Group of Institutions, Unnao, India.

Mahipal Singh Choudhry at el., "*MRI Brain Image Classification using Polynomial Kernel Principal Component Analysis with Neural Network*", International Journal of Advance Technology in Engineering and Science (ISSN 2348-7550), 2016, Vol: 04, no: 03, pp: 39-46.

TABLE OF CONTENTS

LIST OF FIGURES

LIST OF TABLES

CHAPTER 1

INTRODUCTION TO BIOMEDICAL SIGNALS PROCESSING

Firstly different types of biomedical signals, like Electrocardiogram (ECG), Electroencephalogram (EEG) and Magnetic Resonance Imaging (MRI), are included in this chapter. Thereafter, biomedical signals processing and challenges in biomedical signals processing, which includes artifacts of ECG and EEG along with challenges in MR image segmentation are described. At last, the problem statement and contribution of the thesis is followed by the significance of the study and the thesis overview.

1.1 Biomedical Signals

Biomedical signals are broadly classified into two major categories as:

- **1-D Biomedical Signal**: 1-D biomedical signals are further classified into three sub-categories as
  - **Biochemical:** In the form of pH changes, hormones and neurotransmitters.
  - **Bioelectrical:** In the form of electrical signals (Potential or Current) like Electrocardiogram, Electroencephalogram, Electromyogram, Electrooculography, Electrogastrogram, and Magnetoencephalogram.
  - **Biomechanical:** In the form of pressure or temperature like Mechanomyogram.
- **2-D Biomedical Signal**: X-Ray, Ultrasonography (USG), MRI, Computed Tomography (CT) Scan and Nuclear Medicine are important 2-D biomedical signals/images.

ECG and EEG are the most important 1-D bioelectrical signals as they measure electrical activities of heart and brain respectively. Magnetic Resonance Imaging (MRI) is one of the most important 2-D biomedical signal or imaging method.

1.2 Electrocardiogram (ECG)

ECG is a quasi-periodic signal, quantifying the electrical activities of the heart and it is used to measure the rate and regularity of heartbeats, as well as the size and position of the chambers, presence of any damage to the heart and effects of drugs or devices used to regulate the heart, such as a pacemaker. It includes information content mostly in the 0.05-120 Hz range and amplitude in the range of 0.02- 5 mV. It primarily consists of P wave, QRS complex and ST segment [1] as shown in Fig 1.1

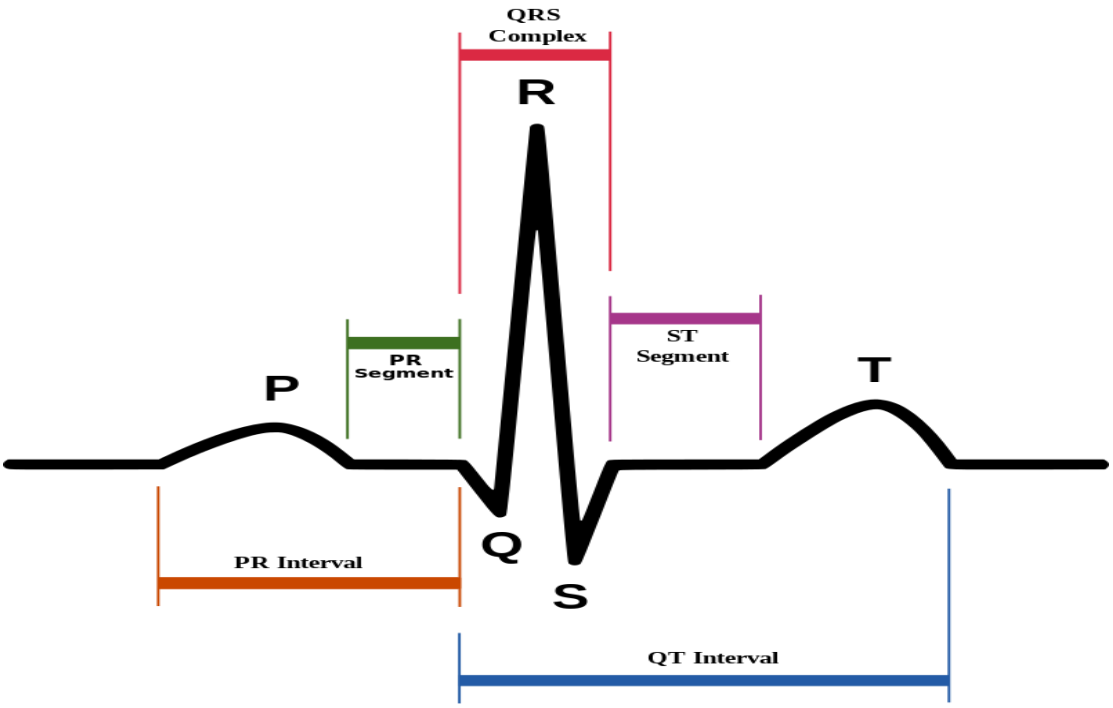

Fig 1.1: Typical ECG Waveform

1.3 Electroencephalogram (EEG)

EEG refers to the recording of the brain's spontaneous electrical activity over a short period of time, recorded from multiple electrodes placed on the scalp with a conductive gel or paste. The EEG spectrum has different frequency sub-bands in the range of 0.1 Hz to 100

Hz. Commonly used sub-bands are **Delta (**0.1 – 4.0 Hz), **Theta (**4.0 – 8 Hz), **Alpha** (8.0 - 14.0 Hz), **Beta (**14.0 - 30.0 Hz) and **Gamma (**30.0 - 100.0 Hz) [2]. EEG sub-bands are shown in Fig 1.2. The x-axis shows normalized frequency with respect to maximum frequency of 4 Hz, 8 Hz, 14 Hz, 30 Hz and 100 Hz for Delta, Theta, Alpha, Beta and Gamma sub-bands respectively.

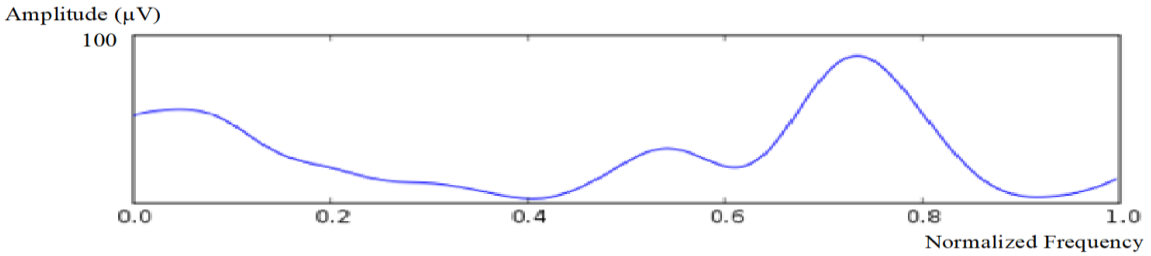

(a) Delta

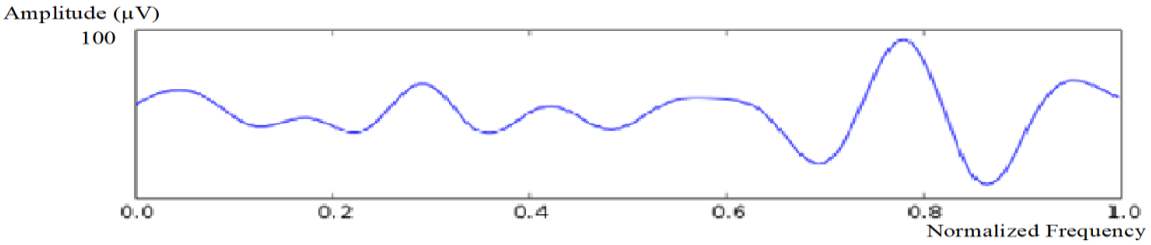

(b) Theta

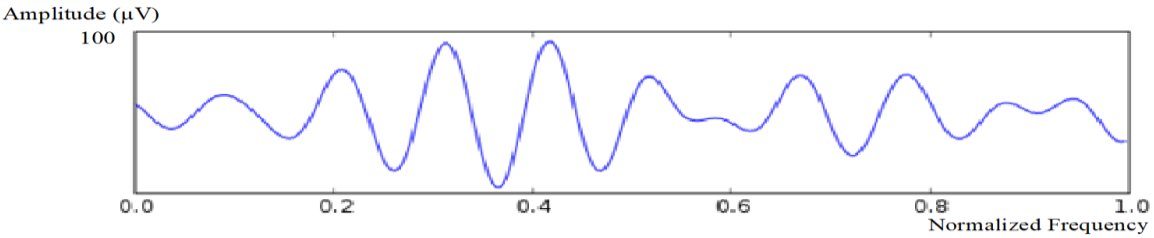

(c) Alpha

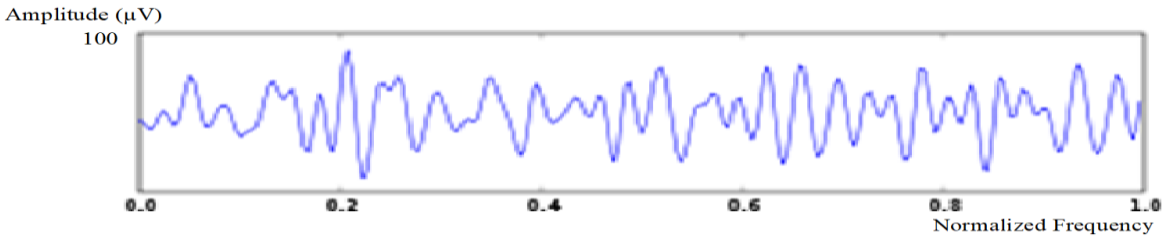

(d) Beta

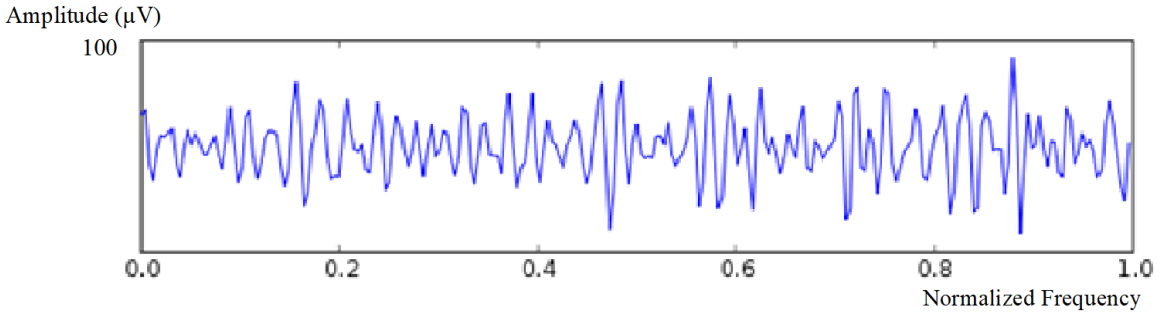

(a) Gamma

Fig 1.2: EEG Sub-bands

EEG has various advantages over other techniques to study the brain functions as it has less hardware cost and due to the absence of radiations or injections, it is considered very safe.

1.4 Magnetic Resonance Imaging (MRI)

Magnetic Resonance (MR) imaging has come up as a widely accepted and revolutionary innovation to provide detail and reliable information in the field of medical imaging. MRI is preferred over other imaging methods for medical imaging purpose because it does not involve any ionizing radiation and is used in non-invasively forms. Segmentation is a critical stage in the investigation of MR images [3].

Image segmentation is a process of assigning a label to every pixel of the image such that pixels with the same label have certain similar characteristics. It divides a digital image into multiple segments, where each segment has the similar type of pixels. The main goal of image segmentation is to simplify and change the representation of an image into a more meaningful and useful form to process it for different purposes.

Image segmentation techniques are broadly divided into two groups; Edge based segmentation and region based segmentation [4]. In edge-based segmentation, regions in an image are divided by running edge detection on the image where the edges are identi-

fied between disjoint segments. In region-based segmentation, the image is taken as a single region and segmentation divides the single region into multiple regions such that the union of all the regions gives the original image and each region is disjoint from each other.

1.5 Biomedical Signal Processing

The biomedical signal processing technique is one of the most important visualizations and interpretation method to support scientific hypotheses and medical diagnoses. Biomedical signal processing aims at extracting significant information from biomedical signals for purposes of diagnosis and evaluating therapy. In some cases, biomedical signal processing techniques are used to interpret physiological signals for designing systems and algorithms for their manipulation.

1.6 Challenges in Biomedical Signal Processing

The processing of biomedical signals poses a set of problems due to the complexity of the biomedical signals and variety of artifacts of biomedical signals. A large number of processing methods and algorithms are available but in order to apply the best method, the user must know the goal of the processing, test conditions and characteristics of the underlying signal. The signal processing method of 1-D biomedical signals mainly deals with artifact removal from the signal. In case of 2-D biomedical signals or images (especially MR images), the focus is on image classification and denoising. Segmentation of MR images is the most important step of image classification and denoising.

1.6.1 ECG Artifacts

ECG signal captures a large number of varying noises during signal acquisition, thereby making proper diagnosis very difficult. Some of these artifacts are Power line interference, Baseline wander, Electrode contact & motion artifact and Instrumentation noise [5].

Source of power line interference is the presence of nearby power line or power supply during ECG. Power line interference has frequency component of 50/60 Hz (Frequency of power supply transmission) or its harmonics. It is in the form of short spikes with amplitude up to 50 % of QRS amplitude.

Electrode metal-to-solution interference and fluctuations in skin potential due to skin stretch are two important sources of electrode contact & motion artifact in ECG. It affects more to lower frequency components (1-10 Hz) of ECG. The amplitude of electrode contact & motion artifact is up to 20% of ECG.

1.6.1.1 Baseline Wander

Baseline wander artifact, which occurs in the low-frequency region of ECG (Generally up to 0.5 Hz but more in case of stress ECG), is one of the most important types of noises present in ECG. It takes place due to the respiration of the patient, thereby making it omnipresent in all ECG signals. This artifact is often found during stress ECG as patient breathing rate increases. The baseline wanders artifact results in a gradual sloping of the ST segment and a reduced R-R duration in the ECG signal [6]. For proper diagnosis of ECG signal, it is necessary to remove the constituent noise while ensuring no loss of information in terms of the morphology of the ECG signal. ECG signals corrupted by various artifacts are shown in Fig 1.3 as

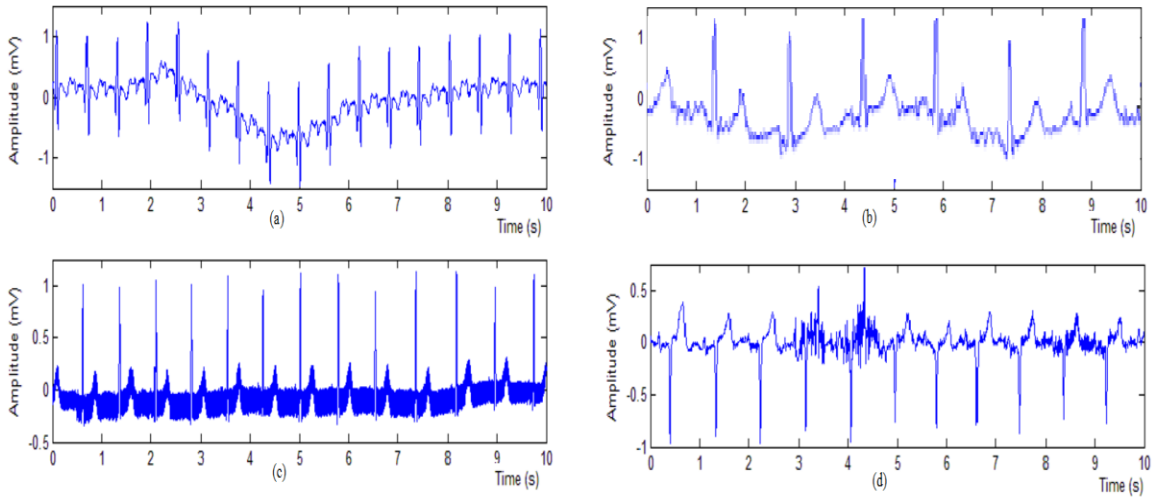

Fig 1.3 ECG signal corrupted by (a) Baseline wander (b) Motion artifact (c) Power line interference (d) Electromyographic noise

1.6.2 EEG Artifacts

The EEG artifacts can be divided into classes of patient-related (physiological) artifacts and system artifacts. Common patient-related or internal artifacts are Electro-Myogram (EMG), ECG or pulsation, Electro-Oculogram (EOG) or Ocular artifact, ballistocardiogram and sweating. The system or external artifacts are 50/60 Hz Power supply interference, Impedance fluctuation, Cable defects, Electrical noise from the electronic components and unbalanced impedances of the electrodes.

1.6.2.1 Electro-Oculogram (EOG) or Ocular Artifact

The ocular artifact is the most common artifact in EEG. The main cause of EOG artifacts is eye movement and eye blinks during EEG recording. A significant potential difference occurs between the cornea and the retina due to blinking which affects the EEG recording [7]. Ocular artifact affects more to the low-frequency region (up to 16 Hz) of EEG.

1.6.3 Challenges in MR Image Segmentation

Image segmentation is one of the most important tasks in medical image analysis and it is the first and the most critical step in many clinical applications. Graph Partitioning, Region Growing, Split and Merge, k-means clustering, Thresholding, Histogram and FCM are commonly used for MR image segmentation [3]. FCM clustering is one of the most admired methods in medical image segmentation because of its fuzzy nature, where one pixel can belong to multiple clusters and leads to better performance than crisp methods [8]. Noise and intensity inhomogeneity make segmentation of images challenging, especially for medical images.

1.7 Problem Statements

Diagnosis of baseline wander artifact and other artifacts are performed by the presence of certain morphologies in the ECG signal. Thus the morphology of an ECG signal is a cru-

cial aspect. Most of the existing ECG denoising methods generally results in loss of information due to change in morphology of an ECG signal. A new method is proposed for baseline wander artifact removal from ECG using cascade combination of Complete Ensemble Empirical Mode Decomposition (CEEMD) and morphological functions with adaptive Structure Elements (SEs). Morphological functions with adaptive Structure Elements (SEs) maintain morphology of ECG during denoising.

A new method is proposed for ocular artifact removal from EEG using the concept of Independent Component Analysis (ICA) and Stationary Wavelet Transform (SWT). Proposed SWT Enhanced ICA method sustains morphological information present in EEG. A novel threshold technique is used in the proposed method to overcome limitations of existing threshold techniques and to make denoising more efficient.

A novel fuzzy energy based level set method obtained by integrating active contour and FCM clustering is proposed for image segmentation of MR images to deal efficiently with noise and intensity inhomogeneity problems. Proposed method effectively deals with intensity inhomogeneity of medical image using FCM based energy function while noise removal from MR images is done using a proposed mean filter based spatial term with energy function.

1.8 Main Contribution of the Thesis

The main contribution of this thesis is to propose new methods for ECG and EEG denoising with the aim that the morphological information present in the 1-D biomedical signal remains preserved. Denoising performance of the proposed method for ECG is independent of heart rate and external factors, especially in the case of stress ECG. Intensity inhomogeneity is a big issue in the case of biomedical images and quality of these images is further degraded in the presence of noise. The proposed method for MR image segmentation simultaneously deals with intensity inhomogeneity and noise in MR image.

1.9 Significance of the Study

The core finding of this study leads to the effective denoising of important biomedical signals (ECG and EEG) and segmentation of biomedical images. Efficient image segmentation, which is an important part of image denoising, significantly contributes to the efficiency of biomedical image denoising and classification. Effective denoising of biomedical signals and images improves quality of significant information extraction from biomedical signals for purposes of signal analysis, diagnosis and efficient system designing.

1.10 Thesis Overview

In Chapter 2, the details of the earlier state-of-the-art methods with their merits and demerits are described. It also highlights research gaps in the concerned area and based on the research gaps, the objectives of the research are formulated.

Chapter 3 includes details of the proposed method for baseline wander removal from ECG. The proposed method is explained in detail with results and significant findings.

A new method for ocular artifact removal from EEG is explained in Chapter 4. Independent Component Analysis (ICA), Stationary Wavelet Transform, the proposed novel thresholding technique, results and significant findings are discussed in detail in this chapter.

Chapter 5 includes details of the proposed method for MR image segmentation. Different steps of the proposed method like local region based energy function using FCM, two-phase and multi-phase level set formulation, equation updation and spatial term for reducing noise effect, are discussed in this chapter with results and significant findings. Chapter 6 highlights important conclusions drawn from the research and also includes details of the future scope of work. .

CHAPTER 2

LITERATURE REVIEW

This chapter contains the details of earlier work carried out for baseline wander removal from ECG, ocular artifact removal from EEG and MR image segmentation methods, with their merits and demerits.

2.1 Baseline Wander Removal from ECG

Earlier state-of-the-art methods for baseline wander removal from ECG can be classified into four categories of Adaptive Filters, Empirical Mode Decomposition (EMD), Ensemble Empirical Mode Decomposition (EEMD) and Morphological Functions.

2.1.1 Adaptive Filter

Initial techniques of baseline wander denoising from ECG signals have used digital window based filters [9] [10] for the removal of low-frequency noise from ECG. As an improvement upon window based filters, different adaptive filters [11] [12] [13] are used for ECG denoising.

An adaptive filter is a system with linear filter. The transfer function of the filter is controlled by variable parameters and it has a mean to adjust these parameters according to an optimization algorithm. These filters involve dynamic tracking of the signal and estimation of noise based on the difference between the tracked signal and the observed one.

2.1.2 Empirical Mode Decomposition (EMD)

EMD decomposes a signal into Intrinsic Mode Functions (IMF) corresponding to various frequency components of the signal. EMD has been found to be very effective in ECG

denoising and has been extensively used in several algorithms [14] [15] [16]. However, most of the work using EMD has been done for the removal of high-frequency noises. EMD is used for the denoising of baseline wander by removing residue to correct the noise signal [18]. Further work in this field is done by decomposing ECG signal into 15 IMF and the baseline wander is removed by dropping last three components [19].

Different wavelet-based techniques are also used for ECG denoising [20] [21] [22]. A combination of EMD and wavelets [23] is a very effective technique for ECG de-noising. All these techniques are generally applied to deal with the lower IMFs or high-frequency components present in the signal henceforth can't be used effectively to deal with baseline wander [24].

2.1.3 Ensemble Empirical Mode Decomposition (EEMD)

To overcome limits of EMD, a system of Ensemble Empirical Mode Decomposition (EEMD) [25] [26] is used for denoising of ECG [27]. In case of EEMD, an ensemble of the original signal is taken by adding various instances of Gaussian white noise to it and these instances are then broken down using EMD and then average over the entire ensemble is taken.

2.1.4 Morphological Functions

In case of the biomedical signal, the morphological operators are used the first time for denoising of EKG signal. Opening and closing operators are used first time for ECG de-noising [28]. The opening operator is used to extract positive pulses, while the closing operator is used to remove the negative waves. The primary drawback of this approach is that an ECG like but not pure ECG signal is analyzed. Further, the use of a disk-shaped structuring element (SE) is a poor approximation for a real ECG [29].

In some more recent approaches [30] [31] for use of morphological functions to handle baseline wander, the morphologies present in the ECG signals are removed in two steps by using opening and closing operations and then by taking the average. Firstly, the QRS complex is removed and then P and T pulses are removed. Linear structuring elements are used in accordance with the available biological data.

2.1.5 Research Gaps

Digital window based filters, when used for baseline removal from ECG, introduce ripples in pass band if a sharp cut-off is opted [32]. This ripple changes the morphology of the ECG signal, which is unacceptable from a diagnosis point of view. Furthermore, inability to effective use of Fourier Transform on ECG signal due to its non-stationary and non-linear property, implies uncertainty about exact frequency cut-offs requirement of window based filters.

The problem that arises while using adaptive filters for ECG denoising, begins with the requirement of pure input samples to obtain an estimate of the way the signal changes. Further issues arise due to the mean square error criterion for adaptive filters and also due to the fact that the reference signals are not correlated very well with the primary input [11]. These filters have improved performance compared to simple window-based filtering but still, there is a considerable scope for further improvement.

Problems, arise in the work related to the use of EMD for baseline removal, are due to the lack of a proper system to find out the number of noise affected IMFs. Noise sensitivity and EMD's property of oscillation, aliasing and mode mixing, introduce error in signal [33].

EEMD resolves most of the problems of EMD but it has insufficient denoising capability of baseline wander removal from ECG due to computational complexity and reduction in amplitude of IMF [34]. The major limitations of morphological functions, in

case of baseline removal from ECG, are due to the fact that the ECG signal, being a quasi-periodic and dynamic signal, don't have fixed pulse widths so a more adaptive structuring element is required [35]. This problem is especially observed in the case of stress ECG. There is an inherent baseline drift, an upward slope in the ST interval and a clear change in the lengths of the QRS and ST segments in case of stress ECG.

2.2 Ocular Artifact Removal from EEG

Earlier state-of-the-art methods for ocular artifact removal from EEG are classified in four categories of Discrete Wavelet Transform (DWT), Stationary Wavelet Transform (SWT), Independent Component Analysis (ICA) and Wavelet Enhanced ICA (wICA).

2.2.1 Discrete Wavelet Transform

Discrete Wavelet Transform (DWT) is used for ocular artifact removal from EEG [36] [37]. In these cases of ocular noise removal, hard thresholding is preferred over soft thresholding because ocular artifact occurs for short time duration and soft thresholding modifies the entire signal. Since ocular artifact has significant components in 0-16 Hz so thresholding is desired only to those sub-bands lying in the frequency region of 0-16 Hz. DWTs don't product effective baseline denoising due to shift variance problem of DWT.

2.2.2 Stationary Wavelet Transform

Shift variance problem of DWT can be avoided by using un-decimated DWT, i.e. Stationary Wavelet Transform (SWT) [38]. Many SWT based methods have been proposed to remove ocular artifacts from EEG [39] [40]. SWT is preferred because of time invariance property. In case of SWT, there is no down sampling so no time information is lost and it produces smoother results in low-frequency bands. Soft thresholding functions are not preferred in these cases as continuous derivatives are required for minimum condition

criteria calculation. A modified version of soft thresholding, known as soft-like thresholding, is applied for optimal noise removal.

2.2.3 Independent Component Analysis (ICA)

In ICA based methods [41] [42], used for ocular artifact removal from EEG, independent components and mixing matrix are estimated. Thereafter, artifactual sources are identified using IC marker. Column corresponding to artifactual independent components are made zero in estimated mixing matrix and in the last step, estimated sources are mixed by multiplying them with modified estimated mixing matrix.

2.2.4 Wavelet Enhanced Independent Component Analysis (wICA)

In wICA based method [43], used for automatic noise removal of the ocular artifact, independent components and mixing matrix are estimated using extended infomax ICA. Sample entropy and kurtosis are calculated for each independent component. The threshold value for sample entropy and kurtosis [44] is calculated to identify the artifactual source and then DWT with hard thresholding is applied on the artifactual source. Denoised ECG signal is obtained by multiplying independent components with estimated mixing matrix.

2.2.5 Research Gaps

The efficiency of DWT based methods is restricted due to shift variance and aliasing issue of DWT [45]. Shift variance perturbs wavelet coefficients in the form of oscillation because of the small shift in the signal. Due to discrete time decimation at each stage of DWT with non-ideal filters, aliasing comes into the role. Inverse DWT overcomes this issue only if there is no modification in wavelet coefficients. But wavelet coefficients get modified whenever thresholding is applied. SWT produces smoother results in low-

frequency bands by suppression of ocular artifact but EEG signal is also suppressed, which results in information loss [46].

To apply ICA on EEG signals some assumptions are made like cerebral signal and artifact signal are linearly combined and are statistically independent, the number of recording channel must be greater or equal to the number of independent sources and finally delay because of propagation through mixing medium is insignificant. The efficiency of proposed method depends upon these assumptions and it is very difficult to meet these assumptions for real EEG.

Proposed wICA method does not affect the non-artifactual region as it uses hard thresholding for DWT denoising but results are not optimal due to shift variance issue of DWT [45] and again hard thresholding makes zero to all undesired parts of the signal, which introduces some discontinuities.

2.3 MR Image Segmentation

Earlier state-of-the-art methods for MR image segmentation are classified into categories of active contour models, level set with active contour models and level set approach with FCM based methods.

2.3.1 Active Contour Model

Active contour models are proved to be very effective to distinguish the boundaries of medical images. Active contours also referred as snakes, are used to extract objects by applying the concept of curve evolution. The energies used in these models are such that they are minimized when the curves evolve at the borders of the required object. Usually, these energies have two main components; internal energy and external energy. Internal energy makes the evolving curve smooth and regularizing it and external energy guides the motion of the curve towards its optimal position [47] [48] [49] [50] [51].

2.3.2 Integration of Level Sets Approach with Active Contour Model

A region-based approach is proposed to approximate an image using a piecewise smooth model of it [52]. In this approach, energy term is minimized when the approximation contains smooth regions as well as the sufficient number of edges, they can model the given image. In a similar model, a piecewise constant approximation of an image is obtained instead of the piecewise smooth approximation. The required approximation of the image is achieved using a level set model. The multiphase extension of it is also proposed for image segmentation [53].

Many new methods [54] [55] are proposed by integration of level sets approaches with edge-based active contour models for image segmentation. These proposed methods include an energy term based on edge information into a level set model, which normally utilizes curvature motion.

2.3.3 Integration of Level Sets Approach with Fuzzy C-Means

Fuzzy C-Means clustering membership function is used to overcome initialization problem of proposed methods by integration of level set approach with active contours. The membership function is used to select the parameters required in the level set model. Local intensity clustering property is used for forming a new FCM based clustering [56]. In a modified method [57], the concept of fuzziness has been utilized by integrating FCM_S1&S2 (Spatial based extensions of FCM) and level set model. This model successfully segments images with high noise.

2.3.4 Research Gaps

Snake models are implemented based on parameterized approaches, which face a lot of complexities. The active contour models make an automatic search for their minimum

energy positions, but sometimes they may settle at a local minimum which makes them less effective [58] [59].

Proposed methods for medical image segmentation by integration of level sets approaches with edge-based or region-based active contour models, suffer from limitations of the corresponding edge-based or region-based model. The region-based model depends less on initial level set but edge-based models commonly suffer from the problem of level set initialization. These methods give good results in case of intensity inhomogeneity problem of biomedical images but cannot deal efficiently with noise [56].

Integration of FCM clustering membership function with level sets approach deals efficiently with intensity inhomogeneity and noise individually but cannot effectively deal simultaneously with intensity inhomogeneity and noise in MR images [60].

2.4 Research Objectives

The main objective of this thesis is to analyze various issues involved in biomedical signals processing techniques. It is almost impossible to cover all biomedical so two most important 1-D biomedical signals, ECG and EEG, are selected along with MR images (most important 2-D biomedical signal) for this research work. Denoising of biomedical signals is the very critical issue so this research work is focused on it.

Baseline wander is the most common artifact of ECG and ocular artifact is the main source of noise in EEG so they are selected for denoising purpose. Segmentation is a very important step in MR image analysis and denoising so it opts here for this research work. To fulfill these objectives, following frame of works has been performed

- A new method is proposed for baseline wander removal from ECG
- A new method is proposed for ocular artifact removal from EEG
- A novel frame work is proposed for MR image segmentation.

CHAPTER 3

A NEW METHOD FOR BASELINE WANDER REMOVAL FROM ECG

This chapter includes the details of Complete Ensemble Empirical Mode Decomposition (CEEMD), adaptive structuring element (SE) based morphological operators, proposed methodology, results and comparative analysis of results.

3.1 Introduction

A new method using cascade combination of CEEMD and adaptive structuring elements based morphological functions is proposed for baseline wander artifact removal from ECG [61]. It is performed in two stages using CEEMD and morphological functions to ensure that morphological information present in the ECG signal is retained with efficient denoising [62]. The proposed method uses strengths of CEEMD and morphological functions, which is supported by results.

3.2 Proposed Methodology

The workflow diagram of the proposed framework is depicted in Fig 3.1

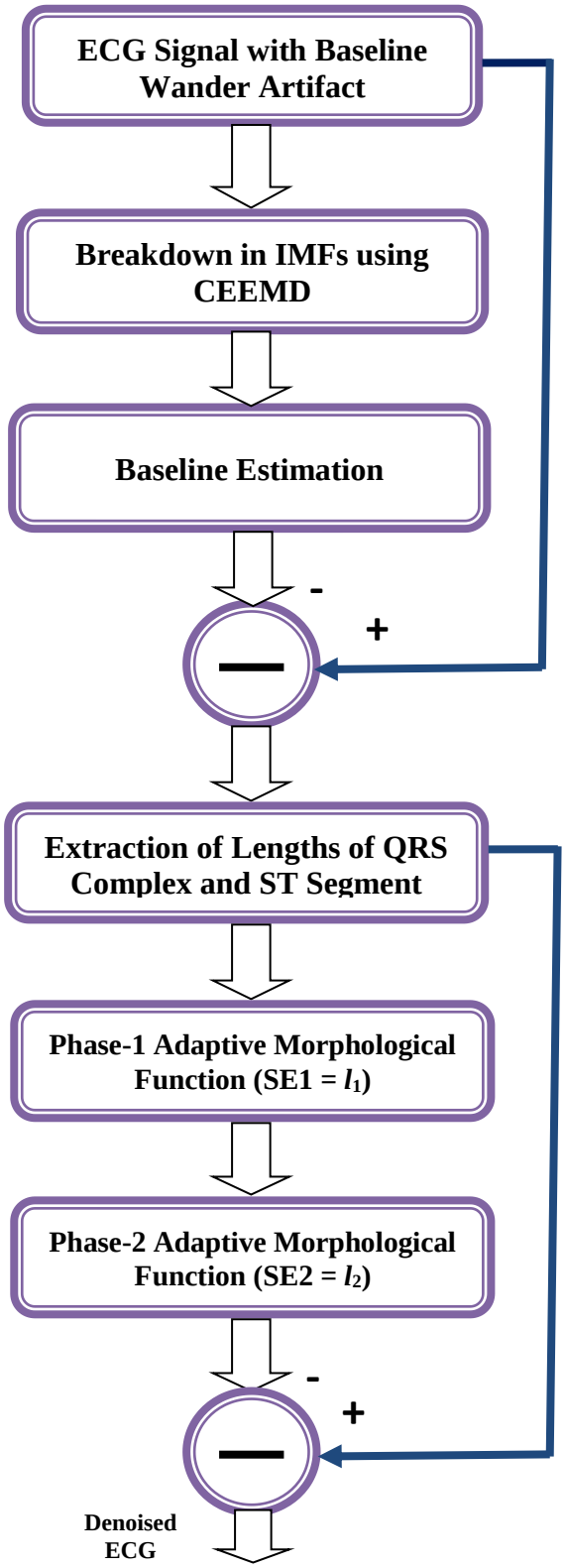

Fig 3.1: Flowchart of the proposed method for baseline wander removal

The proposed algorithm performs denoising in two stages, initially the CEEMD on the noisy signal is performed and a fixed proportion of the total IMFs is subtracted. This partially filtered signal is then applied to a two-step morphological operator based filter with adaptive structuring elements. The morphological filter has been split into two steps, one for QRS complex removal and other to remove ST wave. The morphological filtering is performed in two stages because if all the features are removed at once, it may give rise to severe distortion and loss of information [62]. This cascading of CEEMD and morphological function overcomes the deficiencies of both individual methods.

3.2.1 First Level Baseline Wander Removal

The noisy ECG signal is first decomposed into '***N'*** IMFs (Intrinsic Mode Functions) using CEEMD and then noise dominant '*m*' IMFs (starting from last/highest order IMF) are discarded from ECG signal. This process is performed in following steps: -

i. Raw ECG (ECG signal with Baseline Wander artifact) is decomposed into '*N'* IMFs using CEEMD. IMFs are an indication of the different frequency components present within the signal. Raw ECG signal is written in terms of IMFs as

$$\overline{x}_r(n) = \sum_{i=1}^{N} c_i(n) \quad (3.1)$$

Where $c_i(n)$ is i[th] order IMF. First IMF indicates highest frequency component and last IMF indicates lowest frequency component.

ii. A fraction of N (p; starting from last/highest order IMF) IMFs is discarded from raw ECG. CEEMD filtered ECG signal after discarding last p IMFs is calculated as

$$\overline{x}_c(n) = \sum_{i=1}^{N-p} c_i(n) \quad (3.2)$$

iii. Signal to noise ratio (SNR) of CEEMD filtered ECG signal and Correlation Coefficient (between raw ECG and CEEMD filtered ECG) are calculated using following equations

$$SNR\ (dB)\ = 10 * \log \frac{\Sigma\left(\overline{x}_c(n)\right)^2}{\Sigma\left(\overline{x}_c(n) - \overline{x}_r(n)\right)^2} \tag{3.3}$$

$$r_{xs} = \frac{cov\ (\overline{x}_C(n), \overline{x}_r(n))}{\sigma_{\overline{x}_C}\ \sigma_{\overline{x}_r}} \tag{3.4}$$

Where $\sigma_{\overline{x}_c}$ and $\sigma_{\overline{x}_r}$ are the variances of CEEMD filtered ECG and raw ECG signal (estimated quantities) respectively.

iv. Now the value of discarded fraction (p) is increased and this process (steps ii and iii) is repeated.

It is observed that, on an average, maximum SNR and correlation coefficient are obtained for 'm' discarded IMFs. Value of m is given by

$$m = round\ (0.38\ N) \tag{3.5}$$

Baseline wander estimation at first level is calculated as

$$\overline{x}_{BLW1}(n) = \sum_{i=N-m+1}^{N} c_i(n) \tag{3.6}$$

Partially filtered ECG signal after level 1 ($\bar{x}_1$), is obtained by subtracting first level baseline wander estimated artifact from raw ECG as per following equation

$$\bar{x}_1(n) = \overline{x}_r(n) - \overline{x}_{BLW1}(n) \tag{3.7}$$

3.2.1.1 Complete Ensemble Empirical Mode Decomposition (CEEMD)

CEEMD decomposes any signal into a set of true IMFs [63] and obtained IMFs are an indication of the different frequency components present within the signal. In CEEMD, the breakup of a signal into its constituent IMFs is performed in the following manner: -

- Using EMD, K realizations of the base signal (raw ECG in this case) with added White Gaussian noise ($x(n) + \varepsilon\, w^k(n)$) are achieved to obtain their first modes and thereby to create an ensemble of first IMFs by taking average to obtain first true IMF, using the following formula

$$\widetilde{IMF_1}(n) = \frac{1}{K}\sum_{k=1}^{K} IMF_1^k(n) \tag{3.8}$$

Where $x(n)$ is the base signal (raw ECG signal for the first stage), $w^k(n)$ is White Gaussian noise for k^{Th} realization, $IMF_1^k(n)$ is first IMF of k^{Th} realization, ε is weight coefficient of added noise and $k = 1,2,3,4 \ldots\ldots\ldots\ldots K$.

- At the first stage, the first residue is calculated by

$$r_1(n) = x(n) - \widetilde{IMF_1}(n) \tag{3.9}$$

- For the second stage of CEEMD, this residue signal is considered as base signal and an ensemble of K realizations of the residue with White Gaussian noise is created. First, IMFs for each element are obtained and then they are averaged to have second true IMF, given as

$$\widetilde{IMF_2}(n) = \frac{1}{K}\sum_{k=1}^{K} E_1(r_1(n) + \varepsilon_1 E_1(w^k(n))) \tag{3.10}$$

where E_1 is the mathematical expectation and ε_1 is weight coefficient of the second stage.

- Similar to the above-mentioned equation (3.9), the second residue is calculated and used for third true IMF.
- The above-mentioned steps are continued until further decomposition is no longer possible and all the obtained true IMFs are subtracted from base signal to obtain the final residue, given as

$$r(n) = x(n) - (\widetilde{IMF_1}(n) + \widetilde{IMF_2}(n) + \ldots) \tag{3.11}$$

3.2.2 Second Level Baseline Wander Removal

The partially filtered signal from the first level is now applied to the morphological filters. The morphological filters have been split into two steps with adaptive SEs to avoid distortion in waveform [62].

Structuring element is the most important feature of these filters and by varying the shape and size of the SE, it enables to obtain information from the non-linear system. In the proposed method, linear SEs with an adaptive data-driven length are used. Length of QRS complex and ST interval are used as the length of adaptive SEs for stage 1 and 2 of morphological operators.

A simple algorithm [64], using a wavelet decomposition and identification of ECG components, is used to determine the lengths of QRS complex & ST interval and thereafter, lengths of structuring elements. It is a fully adaptive method in which position of peaks is located and then average length of QRS complex is obtained based on the number of samples between peaks. The length of the QRS complex is defined as the number of samples between the onset of the Q wave and the offset of the S wave. By obtaining the locations of S and T peaks, length of ST interval is calculated. The QRS complex removed ECG signal, from the first stage of the morphological filter, is then applied to the second stage of the morphological filter to remove the ST wave.

Selection of QRS complex and ST interval as adaptive SE length has advantages especially in the case of exercise or stress ECG signals, where due to the external factors (High pulse rate in case of stress ECG), lengths of the QRS complex and ST interval have to be changed [27]. Further, a slope is observed in the ST interval, which must also be removed for accurate diagnosis of cardiac conditions. The data-driven nature of adaptive SE lengths ensure that the filtration algorithm is independent of the nature of ECG being taken; further, it provides far superior filtration in the case of stress ECG.

3.2.2.1 Morphological Operators

Mathematical morphology is a powerful tool for the numerical analysis of geometric structures. It consists of numerous algorithms, designed to obtain information from a geometric object, concerning shape and size of the object. Erosion and Dilation are the fundamental morphological operators, upon which the more advanced processes and filtering techniques are based.

- **Dilation**: Dilation of a point of signal/image $f(x)$ is the maximum of the points in its neighborhood, with that neighborhood defined by the structuring element $g(x)$. Dilation of $f(x)$ by $g(x)$ is given by

$$(f \oplus g)(x) = sup_{y \in B}\big(f(y) + g(x+y)\big) \tag{3.12}$$

  Where sup denotes the supremum and B is the space for that $g(x)$ is defined.

- **Erosion**: Erosion of a point of signal/image $f(x)$ is the minimum of the points in its neighborhood, with that neighborhood defined by the structuring element $g(x)$. Erosion of $f(x)$ by $g(x)$ is given by

$$(f \ominus g)(x) = inf_{y \in B}\big(f(x+y) - g(y)\big) \tag{3.13}$$

  Where inf denotes the infimum.

Two important operations known as opening and closing [65], derived from the erosion and dilation operators, are used in the proposed method and are defined as

$$Opening: (f \circ l)(n) = \big((f \ominus l) \oplus l\big)(n) \tag{3.14}$$

$$Closing: (f \bullet l)(n) = \big((f \oplus l) \ominus l\big)(n) \tag{3.15}$$

Opening operation is defined as erosion followed by dilation. It is responsible for the removal of peaks and smoothening of the contour. Closing operation is defined as the dilation followed by erosion. It handles removal of pits and discontinuities.

The partially filtered ECG signal after level 1 ($\bar{x}_1(n)$), is now applied to the first stage of the morphological filter. Based on the length of a QRS complex, obtained from the real- time ECG signal, a linear structuring element (SE1) of length 'l_1'is used. QRS complex removed ECG signal is given by

$$\bar{x}_{mp1}(n) = \{(\bar{x}_1 \circ l_1 \bullet l_1)(n) + (\bar{x}_1 \bullet l_1 \circ l_1)(n)\}/2 \tag{3.16}$$

The QRS complex removed ECG signal is then applied to the second stage of morphological function, intended to remove the ST wave. ST interval of partially filtered ECG signal is used as the function of the length of structuring element (SE2) for the second morphological filter (l_2). ST segment removed ECG signal is given by

$$\bar{x}_{mp2}(n) = \{(\bar{x}_{mp1} \circ l_2 \bullet l_2)(n) + (\bar{x}_{mp1} \bullet l_2 \circ l_2)(n)\}/2 \tag{3.17}$$

This signal does not contain any of the characteristic ECG segments. It is an estimate of the total remaining baseline noise present in the original signal. This obtained noise signal is subtracted from partially filtered ECG signal after level 1 ($\bar{x}_1(n)$) to achieve clean or denoised ECG signal, which is given by

$$x_{denoised}(n) = \bar{x}_1(n) - \bar{x}_{mp2}(n) \tag{3.18}$$

3.3 Results

The proposed method is tested over a wide range of data taken from synthesis as well as real-time ECG signals. The simulated ECG signal, sampled at 512 Hz and available in MATLAB R2011b, is used to derive the results for the synthetic ECG. In order to increase similarity of synthesis ECG to real-time ECG signal, it is passed through a 9th order Savitzky Golay filter to provide smoothing. Further to simulate baseline wander, different types of low-frequency noises components are added.

Real-time signals are taken from ECG-ID databases [66] [67]. It consists of 310 ECG recordings, obtained from 90 people. Each recording comprises 5000 samples at 500 Hz sampling frequency with 12-bit resolution, for a range of ± 10 mV. Obtained ECG signals are noisy signals containing low-frequency noises.

Performance of proposed method is analyzed in terms of Mean Square Error, Signal to Noise Ratio and Correlation Coefficient using various cascade combinations of EMD, EEMD and CEEMD with different types of morphological operators like static, partially adaptive and fully adaptive. For clean/output ECG signal, performance parameters [35] are calculated as

$$\text{Output Mean Square Error,} \quad MSE = \Sigma\left(x_{original} - x_{denoised}\right)^2 / N \tag{3.19}$$

$$\text{Output Signal to Noise Ratio, SNR (dB)} = 10 * \log \frac{\Sigma\left(x_{original}\right)^2}{\Sigma\left(x_{original} - x_{denoised}\right)^2} \tag{3.20}$$

$$\text{Correlation Coefficient,} \quad r_{x_o\, x_d} = \frac{cov\,(x_{original}, x_{denoised})}{\sigma_{x_o}\, \sigma_{x_d}} \tag{3.21}$$

where, σ_{x_o} and σ_{x_d} are variance of original and denoised signal respectively.

The smaller value of output MSE and larger value of output SNR show better denoising performance. The effectiveness of any method to preserve morphological information present in the ECG signal is verified in term of Correlation Coefficient between original ECG signal and denoised ECG signal. Large Correlation Coefficient shows that proposed method preserves morphological information present in the ECG signal.

Fig 3.2 - 3.4 show plots of baseline wander denoised ECG using EMD, EEMD and CEEMD for three different signals (Recordings). The x-axis shows the number of samples and the y-axis shows the amplitude of the signal. Tables 1-3 show corresponding results of ECG denoising using EMD, EEMD and CEEMD.

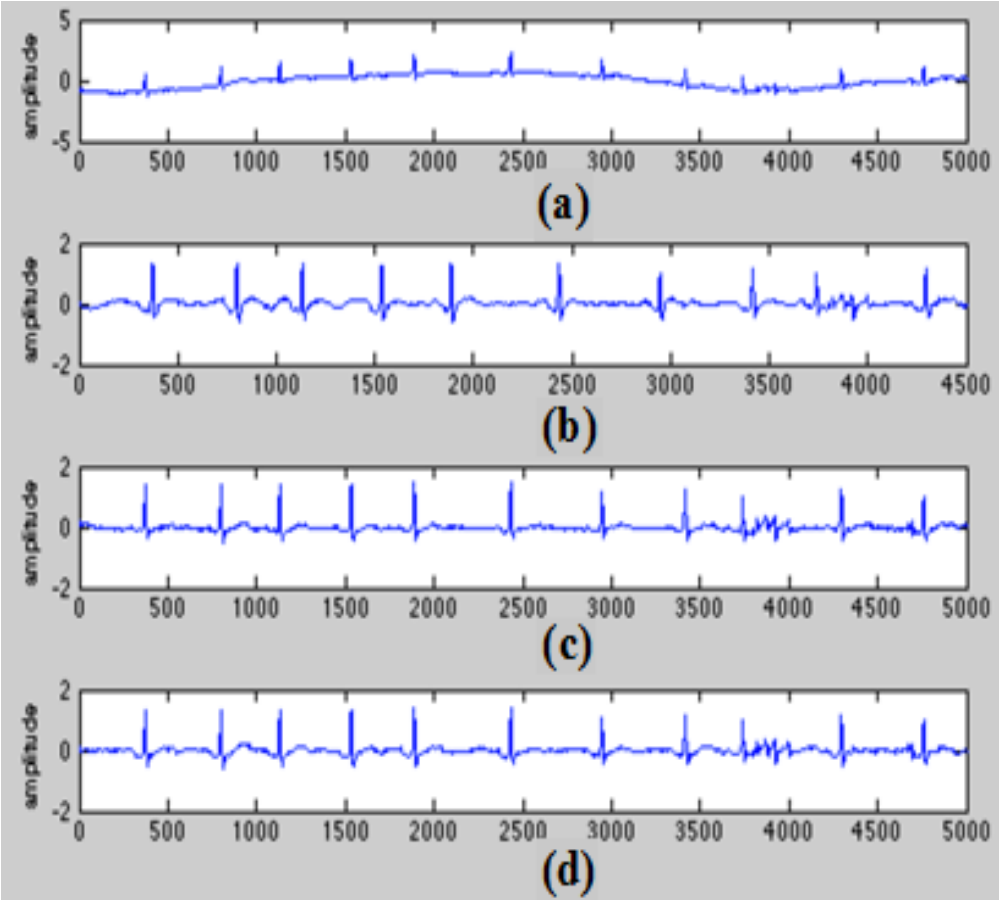

Fig 3.2 (a) Noisy Signal (Recording-1). Denoised signal using (b) EMD (c) EEMD (d) CEEMD

Table 1: Comparison of CEEMD with EMD and EEMD for recording-1 (**Input SNR = 16.286 dB; Input MSE = 0.041)**

	Method		
Parameter	**EMD**	**EEMD**	**CEEMD**
Output MSE	0.015	0.012	0.010
Output SNR(dB)	24.504	26.958	28.541
Correlation Coefficient	0.8582	0.9145	0.9288

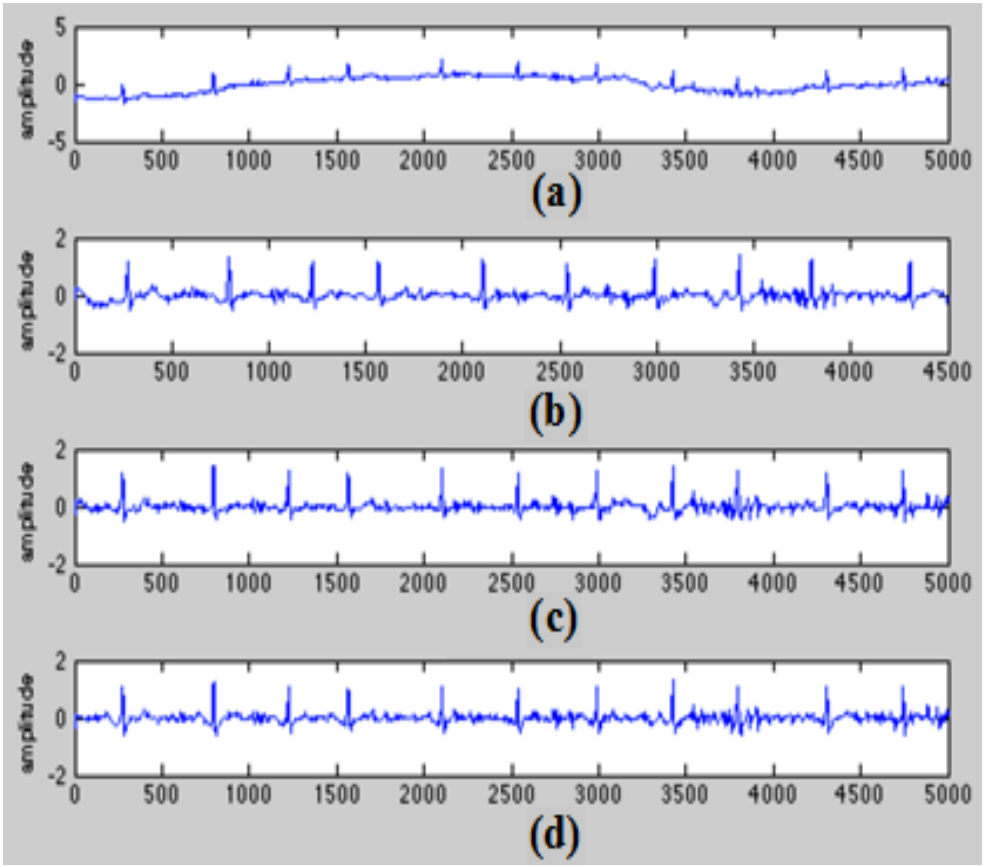

Fig 3.3 (a) Noisy Signal (Recording-2). Denoised signal using (b) EMD (c) EEMD (d) CEEMD

Table 2: Comparison of CEEMD with EMD and EEMD for recording-2 (**Input SNR = 13.176 dB; Input MSE = 0.021)**

	Method		
Parameter	**EMD**	**EEMD**	**CEEMD**
Output MSE	0.007	0.006	0.005
Output SNR(dB)	22.509	23.848	25.431
Correlation Coefficient	0.8598	0.9092	0.9214

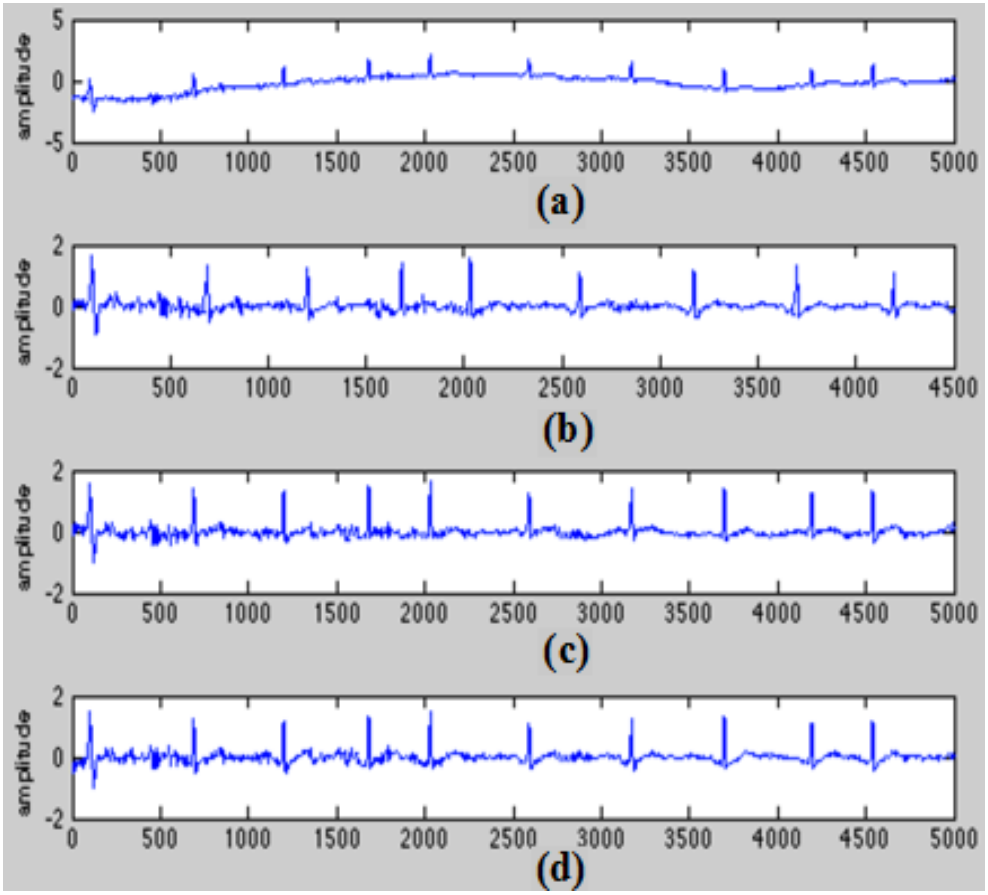

Fig 3.4 (a) Noisy Signal (Recording-3). Denoised signal using (b) EMD (c) EEMD (d) CEEMD

Table 3: Comparison of CEEMD with EMD and EEMD for Recording-3 (**Input SNR = 12.486 dB; Input MSE = 0.041)**

	Method		
Parameter	**EMD**	**EEMD**	**CEEMD**
Output MSE	0.015	0.013	0.010
Output SNR(dB)	21.219	22.462	24.741
Correlation Coefficient	0.8658	0.8998	0.9114

Results show a clear superiority of the CEEMD method over EMD and EEMD and justify the selection of EEMD based filter for removal of baseline wander. Superior denoising efficiency is shown in terms of lower MSE and higher SNR values. Better morphological information retaining capability is proved by larger value of correlation coefficient.

Fig 3.5 - 3.7 show plots of denoised ECG using morphological functions with various levels of adaptiveness for ECG baseline wander denoising for three different ECG signals. The x-axis shows number of samples and the y-axis shows the amplitude of the signal. Tables 4-6 show corresponding results for various levels of adaptiveness of morphological operators.

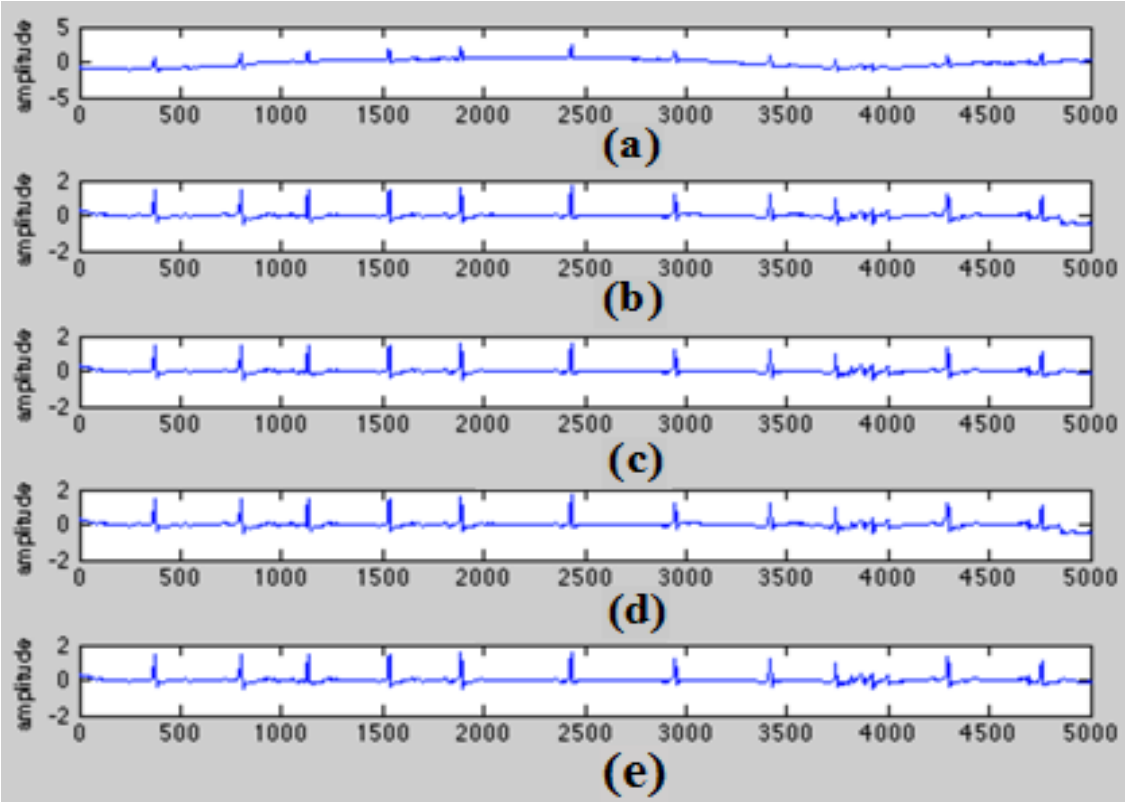

Fig 3.5: (a) Noisy signal (Recording-1). Denoised signal using (b) Static Morphological Operators (c) QRS Adaptive Morphological Operator (d) ST Adaptive Morphological Operator (e) Fully Adaptive Morphological Operators

Table 4: Comparison between different types of morphological functions (MF) for Recording-1 (**Input SNR = 16.286 dB; Input MSE = 0.041)**

	Method			
Parameter	**Static MF**	**Partially Adaptable MF-1 (SE1 = l_1)**	**Partially Adaptable MF-2 (SE2 = l_2)**	**Fully Adaptable MFs (SE1 = l_1; SE2 = l_2)**
Output MSE	0.018	0.016	0.015	0.012
Output SNR(dB)	23.436	24.459	25.019	26.958
Correlation Coefficient	0.8895	0.9024	0.9015	0.9481

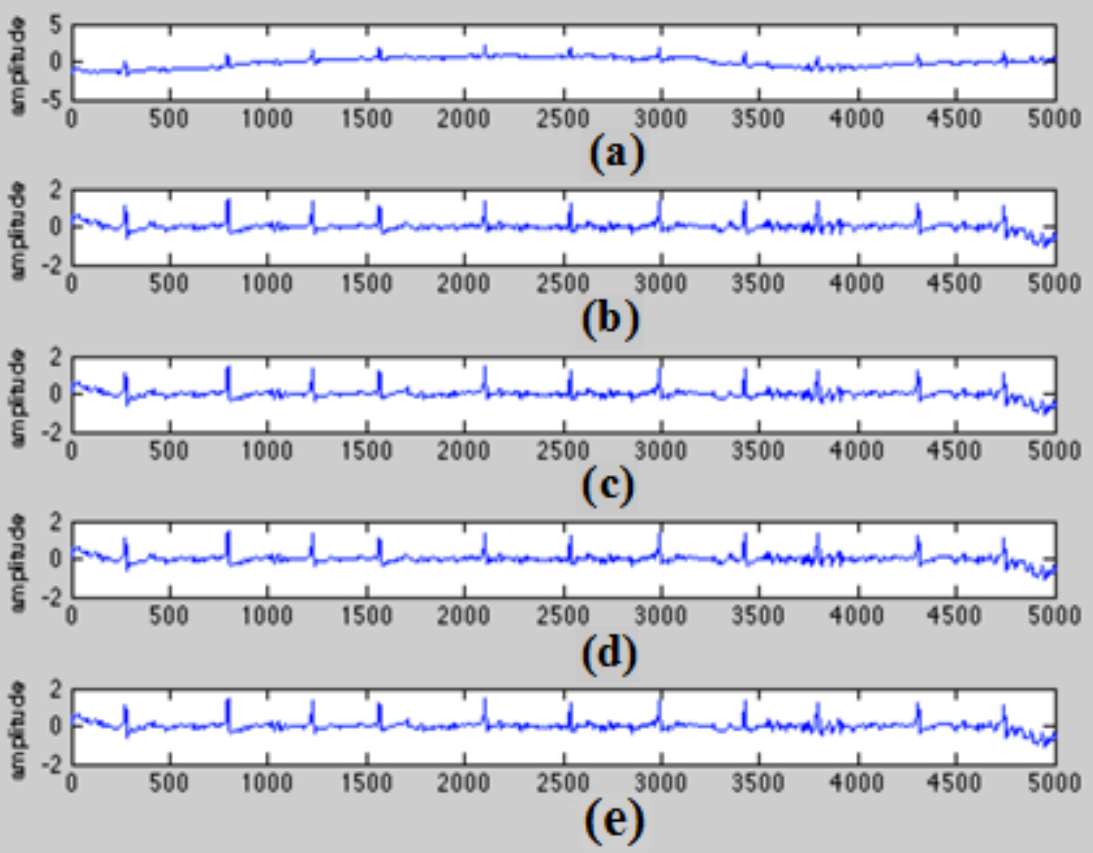

Fig 3.6: (a) Noisy signal (Recording-2). Denoised signal using (b) Static Morphological Operators (c) QRS Adaptive Morphological Operator (d) ST Adaptive Morphological Operator (e) Fully Adaptive Morphological Operators

Table 5: Comparison between different types of morphological functions (MF) for Recording-2 (**Input SNR = 13.176 dB; Input MSE = 0.021)**

Parameter	***Method***			
	Static MF	**Partially Adaptable MF-1 (SE1 = l_1)**	**Partially Adaptable MF-2 (SE2 = l_2)**	**Fully Adaptable MFs (SE1 = l_1; SE2 = l_2)**
Output MSE	0.009	0.008	0.007	0.006
Output SNR(dB)	20.822	21.350	22.509	24.603
Correlation Coefficient	0.8952	0.9176	0.9114	0.9405

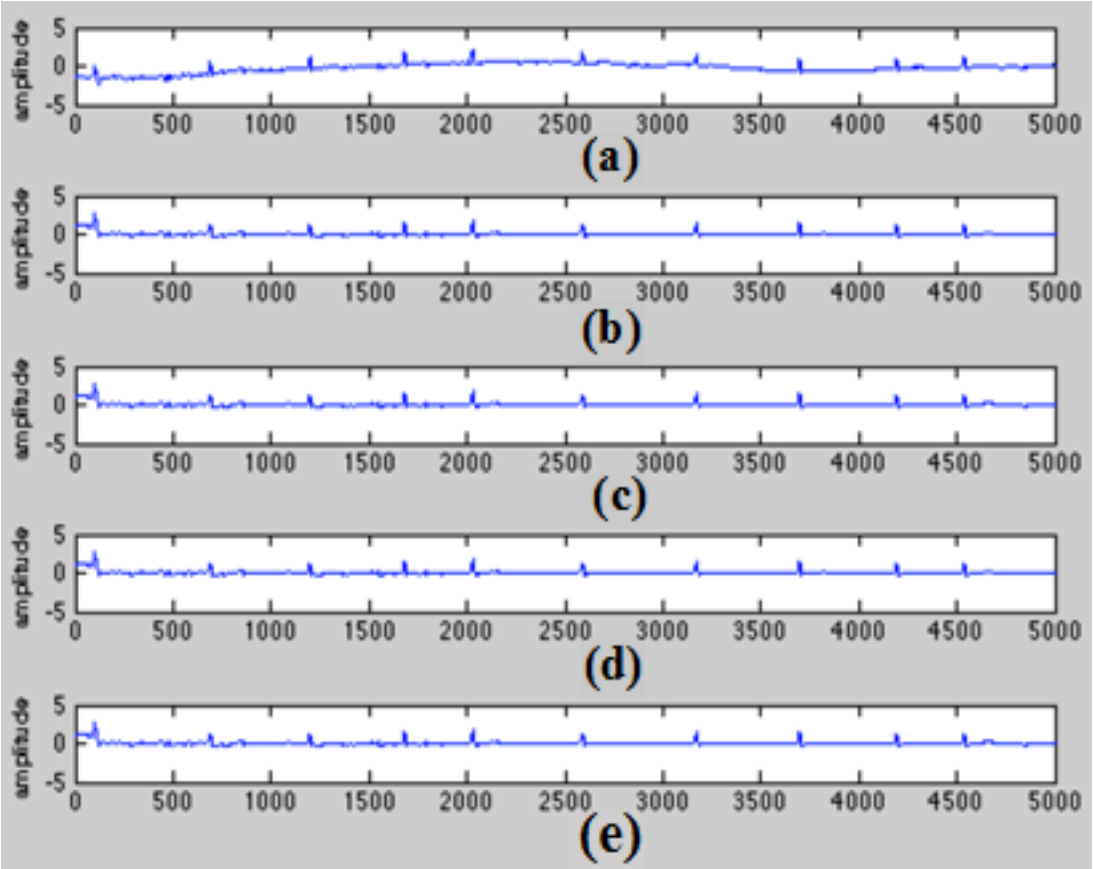

Fig 3.7: (a) Noisy signal (Recording-3). Denoised signal using (b) Static Morphological Operators (c) QRS Adaptive Morphological Operator (d) ST Adaptive Morphological Operator (e) Fully Adaptive Morphological

Table 6: Comparison between different types of morphological functions (MF) for Recording-3 (**Input SNR = 12.486 dB; Input MSE = 0.041)**

Parameter	***Method***			
	Static MF	**Partially Adaptable MF-1 (SE1 = l_1)**	**Partially Adaptable MF-2 (SE2 = l_2)**	**Fully Adaptable MFs (SE1 = l_1; SE2 = l_2)**
Output MSE	0.019	0.017	0.016	0.014
Output SNR(dB)	19.166	20.132	20.660	21.819
Correlation Coefficient	0.9012	0.9155	0.9103	0.9396

The filtering properties change from a static function to one in which the first stage is adaptive, then one in which the second stage is adaptive and finally the fully adaptive model. It can be clearly seen that adaptability enhances the denoising property of filter and fully adaptive filter gives the best results.

Fig 3.8 – 3.10 show plots of baseline denoised ECG using a cascaded combination of CEEMD with morphological functions at various levels of adaptiveness for three different ECG signals. The x-axis shows number of samples and the y-axis shows the amplitude of the signal. Tables 7-9 show corresponding results using a cascaded combination of CEEMD with morphological functions at various levels of adaptiveness.

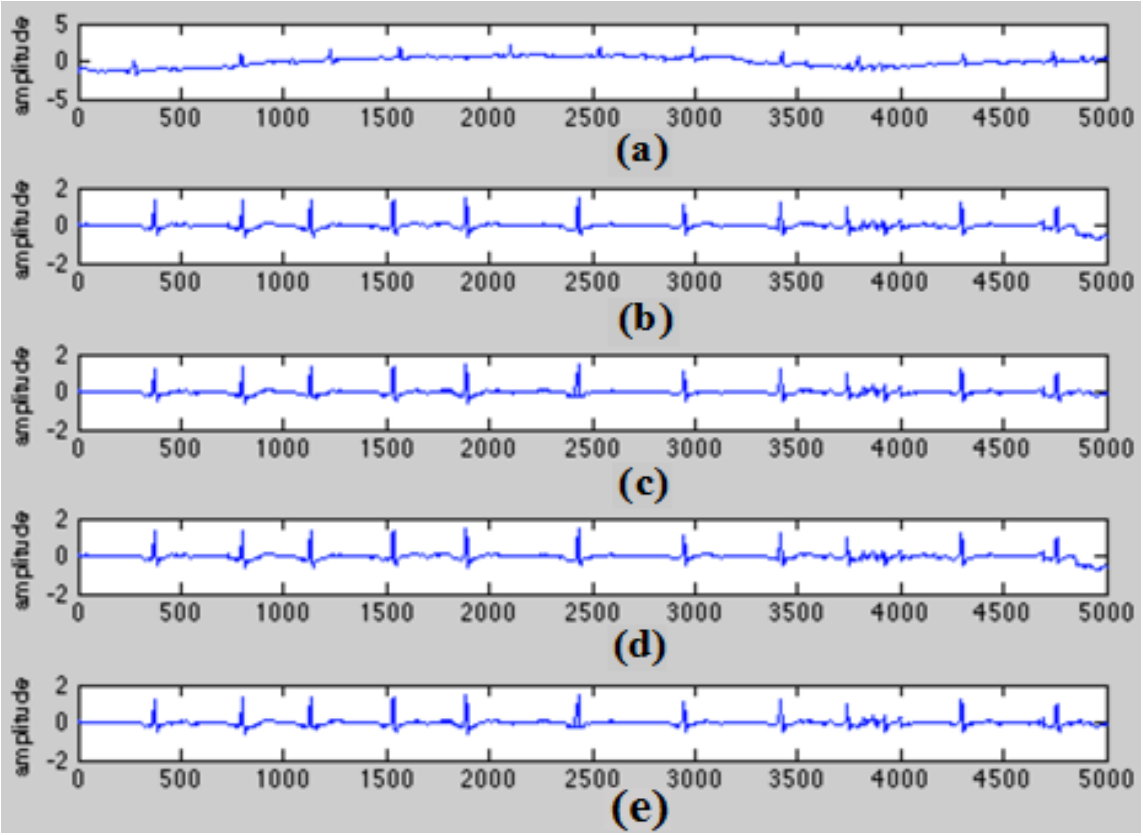

Fig 3.8: (a) Noisy signal (Recording-1) and denoised signal using a cascaded combination of CEEMD with (b) Static Morphological Operators (c) QRS Adaptive Morphological Operators (d) ST Adaptive Morphological Operators (e) Fully Adaptive Morphological Operators

Table 7: Comparison between cascaded combination of CEEMD with different types of morphological functions (MF) for Recording-1 (**Input SNR = 16.286 dB; Input MSE = 0.041)**

	Method			
Parameter	**CEEMD & Static MF**	**CEEMD & Partially Adaptable MF-1 (SE1 = l_1)**	**CEEMD & Partially Adaptable MF-2 (SE2 = l_2)**	**CEEMD & Fully Adaptable MFs (SE1 = l_1; SE2 = l_2)**
Output MSE	0.008	0.006	0.005	0.004
Output SNR(dB)	30.479	32.978	34.562	36.501
Correlation Coefficient	0.9354	0.9572	0.9586	0.9718

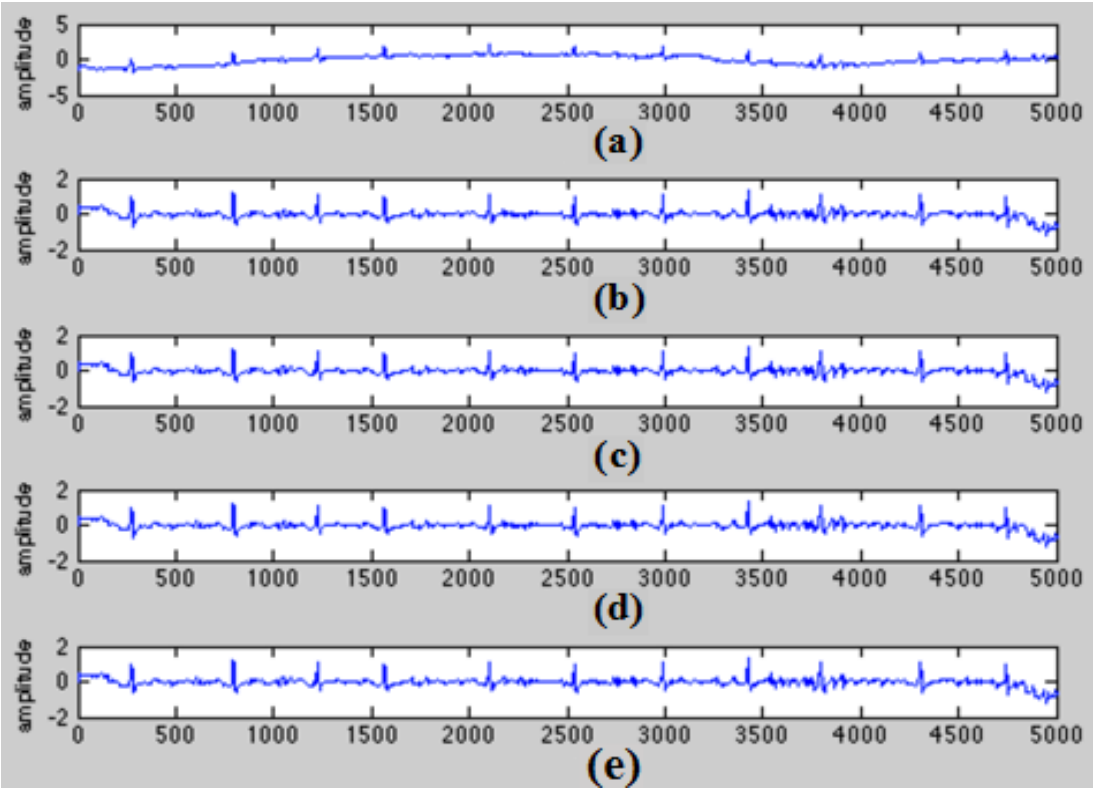

Fig 3.9: (a) Noisy signal (Recording-2) and denoised signal using a cascaded combination of CEEMD with (b) Static Morphological Operators (c) QRS Adaptive Morphological Operators (d) ST Adaptive Morphological Operators (e) Fully Adaptive Morphological Operators

Table 8: Comparison between cascaded combination of CEEMD with different types of morphological functions (MF) for Recording-2 (**Input SNR = 13.176 dB; Input MSE = 0.021)**

	Method			
Parameter	**CEEMD & Static MF**	**CEEMD & Partially Adaptable MF-1 (SE1 = l_1)**	**CEEMD & Partially Adaptable MF-2 (SE2 = l_2)**	**CEEMD & Fully Adaptable MFs (SE1 = l_1; SE2 = l_2)**
Output MSE	0.004	0.003	0.003	0.002
Output SNR(dB)	27.550	30.048	30.244	33.568
Correlation Coefficient	0.9381	0.9602	0.9592	0.9801

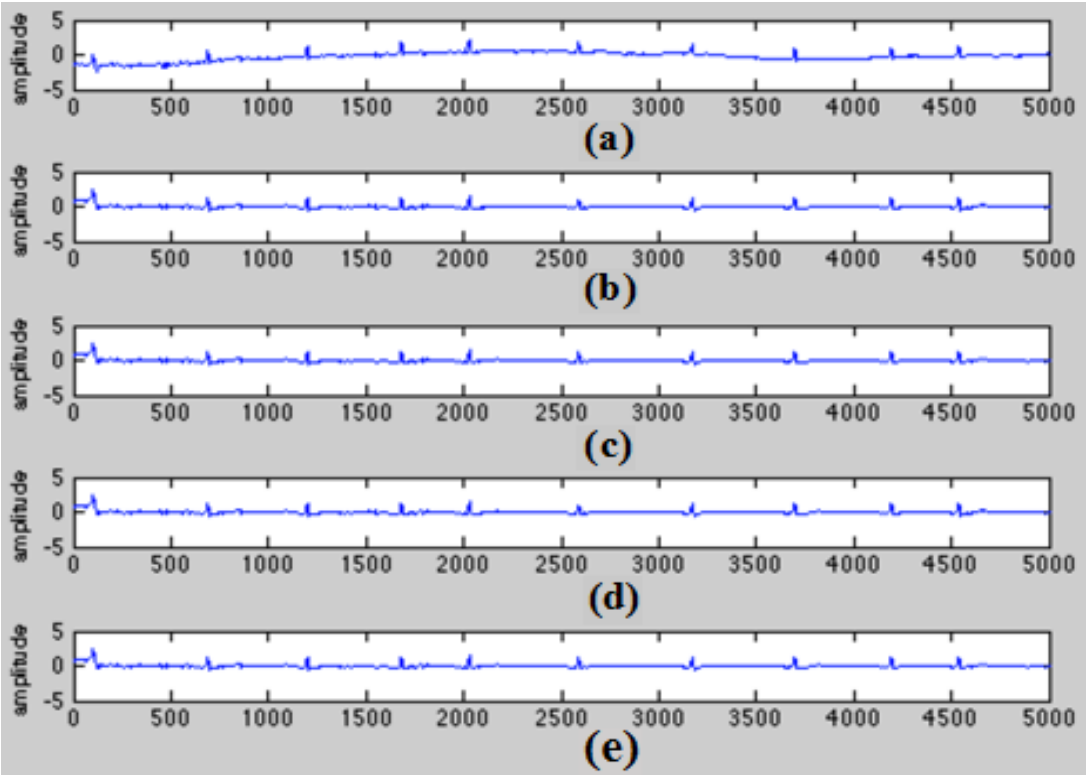

Fig 3.10: (a) Noisy signal (Recording-3) and denoised signal using cascaded combination of CEEMD with (b) Static Morphological Operators (c) QRS Adaptive Morphological Operators (d) ST Adaptive Morphological Operators (e) Fully Adaptive Morphological Operators

Table 9: Comparison between cascaded combination of CEEMD with different types of morphological functions (MF) for Recording-3 (**Input SNR = 12.486 dB; Input MSE = 0.041)**

	Method			
Parameter	**CEEMD & Static MF**	**CEEMD & Partially Adaptable MF-1 (SE1 = l_1)**	**CEEMD & Partially Adaptable MF-2 (SE2 = l_2)**	**CEEMD & Fully Adaptable MFs (SE1 = l_1; SE2 = l_2)**
Output MSE	0.008	0.007	0.006	0.004
Output SNR(dB)	26.678	27.840	28.941	32.462
Correlation Coefficient	0.9204	0.9477	0.9528	0.9812

It can be clearly seen that adaptability enhances the denoising property of filter in cascaded combination also and cascade combination of CEEMD and fully adaptive filter gives the best results.

3.5 Significant Findings

For first level baseline wander removal, CEEMD provides superior result than EMD and EEMD by properly handling oscillation, aliasing and mode mixing problems. For second level baseline wander removal, implementation of two stages morphological function with adaptive SEs provides best results. Denoising efficiency (in terms of SNR and MSE) and morphological information retaining capability (in term of Correlation Coefficient) is further improved by using CEEMD and adaptive morphological function at first and second level respectively. Proposed method effectively removes baseline wander from ECG signal and properly retains morphological information of the ECG signal.

This chapter is based on the following work:

Mahipal Singh Choudhry, Rajiv Kapoor, "*Removal of Baseline Wander from ECG using CEEMD and Adaptive Morphological Function*", Journal of Chemical and Pharmaceutical Science (ISSN: 0974-2115, Scopus index journal with SJR: 0.12), Issue 4, pp: 31-37, October 2016 [61].

CHAPTER 4

A NEW METHOD FOR OCULAR ARTIFACT REMOVAL FROM EEG

This chapter includes the details of Independent Component Analysis (ICA), Independent Component (IC), Stationary Wavelet Transform (SWT), proposed thresholding technique, Modified Multi-Scale Entropy (mMSE), Kurtosis, proposed methodology, results and comparative analysis of results.

4.1 Introduction

A new method, using ICA and SWT, is proposed for ocular artifact removal from EEG signal in such a way that morphological information present in the EEG signal remains preserved. Proposed method [68] incorporates strengths of SWT representation and ICA. Limitations of these methods are minimized by using proposed novel thresholding technique, which further increases denoising of EEG signal. Ocular artifact contaminated EEG signal are selected from standard EEG datasets. Ocular artifact affects more to the low-frequency region of EEG and it is represented by independent noise with non-Gaussian (random) model.

4.2 Proposed Methodology

The workflow diagram of the proposed framework is depicted in Fig 4.1.

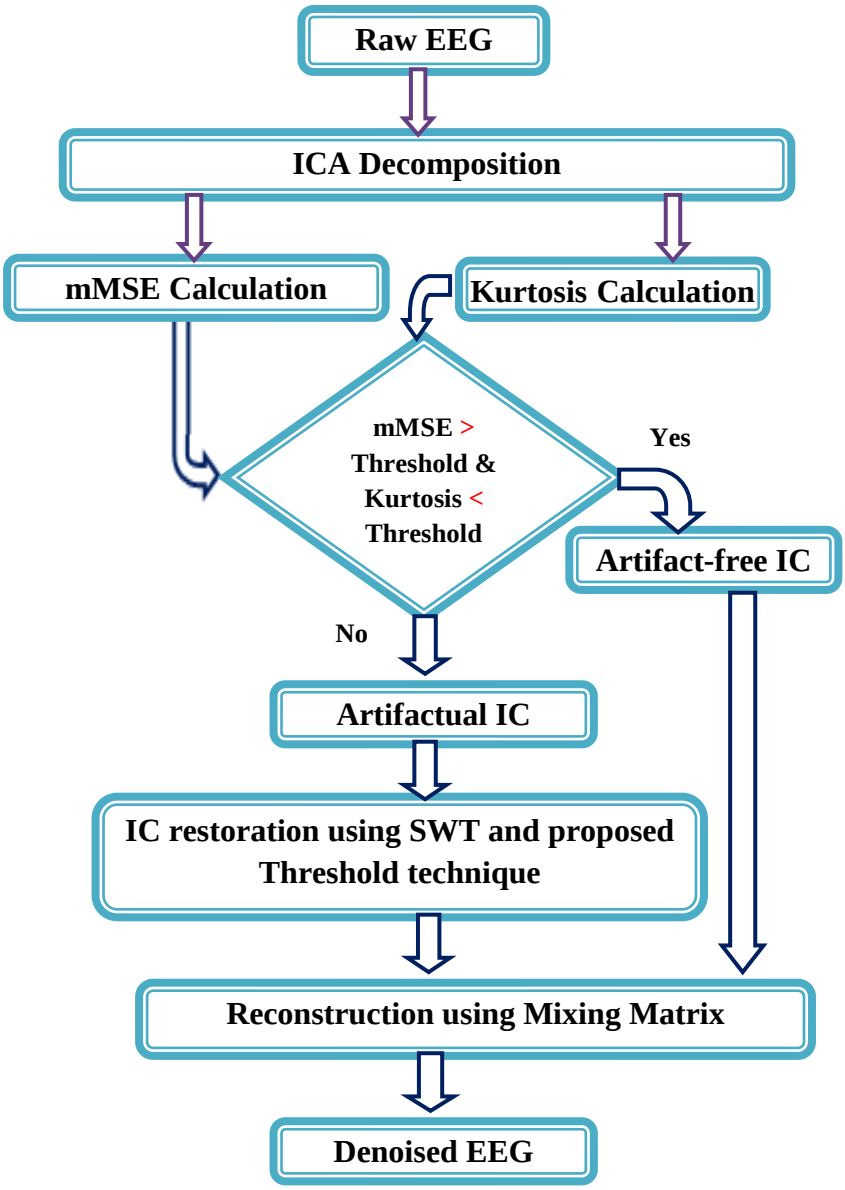

Fig 4.1: Flowchart of the proposed method for ocular artifact removal

The proposed method has following steps:

- ICA decomposition of ocular artifact corrupted EEG.
- Calculation of mMSE and Kurtosis for ICs.
- Separation of artifactual ICs from artifact-free ICs by comparing calculated values of mMSE and kurtosis with their threshold values (Lower limit of the mMSE and upper limit of Kurtosis).

- Restoration of artifactual ICs using SWT and proposed novel thresholding technique.
- Reconstruction of the signal using artifact-free ICs, artifactual ICs after restoration and mixing matrix of ICA.

4.2.1 Independent Component Classification

Ocular artifact corrupted EEG signal is decomposed into ICs using ICA. mMSE and Kurtosis are calculated for all ICs and thereafter, their threshold values are calculated. Artifactual ICs are separated from artifact-free ICs by comparing mMSE and Kurtosis of individual IC with threshold values of mMSE and Kurtosis. ICs having mMSE values, less than the lower limit or Kurtosis value above upper limit, are considered as artifactual components.

4.2.1.1 Independent Component Analysis (ICA)

ICA is a statistical tool, used to decompose a mixed signal (of different recording channels) into independent components (ICs), corresponding to different independent sources [69]. Suppose that an array of channels to provide 'N' observed signals is given by

$$Y = [y_1, y_2, \dots\dots\dots, y_N]^T \tag{4.1}$$

while the ICs corresponding to independent sources are

$$S = [s_1, s_2, \dots\dots\dots, s_N]^T \tag{4.2}$$

Here the assumptions are made that (i) the sources have non-Gaussian distribution and they are mutually statistically independent and (ii) the number of recording channels must be greater or equal to the number of independent sources (or ICs)

The aim of ICA is to decompose the signal into ICs by estimating a demixing matrix W such that

$$S = W \times X \tag{4.3a}$$

where W is defined in such a way that the mutual information is minimized among all ICs in the decomposition process. The mutual information of ICs is defined as

$$I(s_1, s_2, \ldots, s_N) = \sum_{i=1}^{N} H(s_i) - H(x_1, x_2, \ldots., x_N) - \log|\det W| \quad (4.3b)$$

where $\det W$ calculates the determinant of matrix W.

Many algorithms are designed to perform ICA. For sources having super-Gaussian distribution, infomax ICA [70] is the most efficient. The approximate model for raw EEG with the ocular artifact is closest to super-Gaussian distribution so, in the proposed method, infomax ICA is selected among different ICA algorithms.

4.2.1.2 Modified Multi-Scale Entropy (mMSE)

The mMSE analysis is used to evaluate the complexity of a time series by quantifying its entropy over a range of temporal scales. mMSE [71] is implemented by first coarse-graining each IC for multiple scales and then computing the sample entropy for each scale.

For each IC, which is represented by a mono-variate discrete signal $X = \{x_1, x_2, \ldots \ldots \ldots \ldots x_N\}$, mMSE for each IC is calculated [71] as

$$\text{mMSE}\ (m, r) = \log\left(\frac{{B_r}^m}{{A_r}^m}\right) \quad (4.4)$$

where m is the length of patterns that are compared to each other and r is tolerance.

B_r and A_r are the counters to track m and $(m+1)$ template match within the tolerance value r respectively. In terms of template vector pairs, A_r is the number of template vector pairs (of length $m+1$) having distance $d\{X_{m+1}\ (i),\ X_{m+1}\ (j)\} < r$ and B_r is the number of template vector pairs (of length m) having distance $d\{X_m\ (i),\ X_m\ (j)\} < r$.

As per [71] and other, $m = 2$ and r = 2 * Standard deviation of the data sequence of IC.

4.2.1.3 Kurtosis

Kurtosis [72] is a fourth-order statistical parameter, which is used to study the peakedness of distribution of any random variable and is calculated as

$$K = m_4 - 3\,{m_2}^2 \tag{4.5}$$

and

$$m_n = \mathrm{E}\{(x - m_1)^n\} \tag{4.6}$$

where, m_n, m_1 and E are n^{Th} order moment, mean and expectation function of random variable x.

4.2.1.4 Threshold values of mMSE and Kurtosis

The ocular artifact corrupted EEG has the lower value of mMSE compared to pure EEG signal [71]. The signals with peak distribution have higher values of Kurtosis [71] so ocular artifact corrupted EEG has the higher value of Kurtosis compared to pure EEG signal. Threshold values for mMSE and Kurtosis are calculated by using two-sided 95% Confidence Interval (CI) of the mean for t-distribution. The threshold value for mMSE (lower limit of 95% CI of the mean) [71] is calculated as

$$Lower\ limit = \bar{x} - \frac{s}{\sqrt{N}}\ X\ t_{N-1} \tag{4.7}$$

The threshold value for Kurtosis (upper bound of the 95% CI of the mean) is calculated as

$$Upper\ limit = \bar{x} + \frac{s}{\sqrt{N}}\ X\ t_{N-1} \tag{4.8}$$

where, $\bar{x}, s$ and N are samples mean, standard deviation and number of ICs respectively. For the two-tailed test with 95% significance level, $t_{N-1} = 2.201$.

4.2.2 Restoration of Artifactual ICs

The artifactual ICs are restored using SWT and proposed novel thresholding technique. After the restoration of artifactual ICs, signal is reconstructed by applying mixing matrix with artifact-free ICs and restored artifactual ICs.

4.2.2.1 Stationary Wavelet Transform (SWT)

SWT is also called un-decimated DWT, i.e. decimators after filters are not applied in SWT. SWT is similar to the DWT except the signal is never sub-sampled and instead, the filters are up-sampled at each level of decomposition. SWT decomposition filter bank [38] is shown in Fig 4.2.

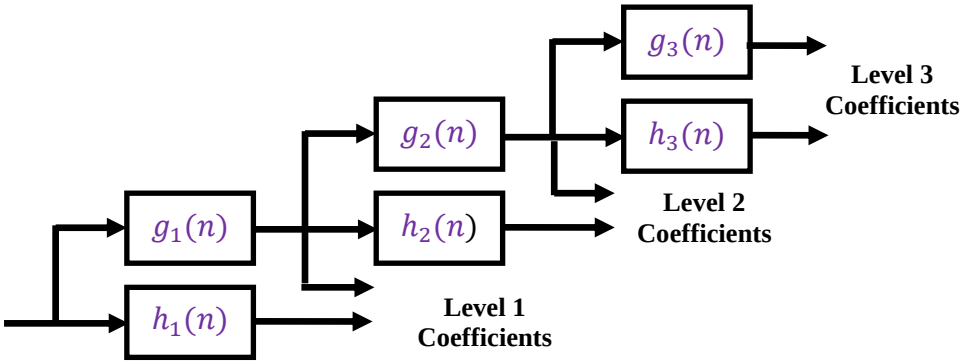

Fig 4.2: 3 Level SWT filter bank

Filters in each level are up-sampled versions of the previous as shown in Fig 4.3.

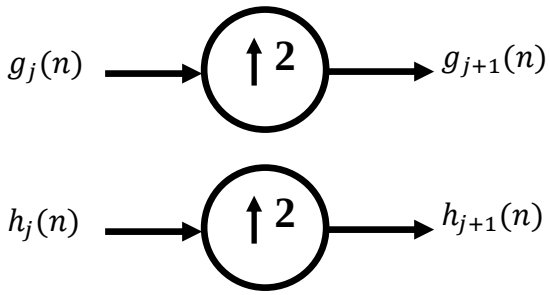

Fig 4.3: SWT filter in different levels

DWT necessitates a decimation by a factor $2N$ (N stands for the level of decomposition) of the transformed signal at each stage of the decomposition. As a result, DWT is not translation invariant which leads to block artifacts and aliasing during the fusion process between the wavelet coefficients. For the SWT scheme, the output signals at each stage are redundant because there is no signal down-sampling; insertion of zeros between

taps of the filters are used instead of decimation. Since there is no down-sampling, it does not lose any time information and have shift invariance property. It also does not suffer from aliasing because no down-sampling is done at any stage. Because of oversampling (up-sampling of filter coefficients by a factor of 2^{j-1} in the j^{th} level of the algorithm), it has very good time resolution for low frequencies and produces smoother results in low-frequency bands.

In the proposed method, SWT with bior-4.4 mother wavelet is used. Decomposition is done up to 6th level and the threshold is applied from 3rd to 6th level of decomposition.

4.2.2.2 Proposed Thresholding Technique

The proposed novel thresholding technique is inspired from hard thresholding. It does not affect the coefficients in the desired range but modifies the coefficients in undesired range (above a threshold value). Hard thresholding in such cases produces undesirable discontinuities [73], while proposed novel thresholding technique is not only suppressing the noise part but also maintaining the smoothness of the signal. Different steps of proposed thresholding technique are as

- The threshold is calculated using any standard risk rule.
- Coefficients are kept unfazed below the threshold value.
- Maxima is calculated for the intervals having values above the threshold.
- Scaling factor for each interval is calculated as follows

$$SF(j) = \frac{d(ind(j)-1)}{max_j} \tag{4.9}$$

  where j denotes j^{th} interval, $ind(j)$ denotes starting index of the j^{th} interval, d denotes interval duration and max_j denotes the maxima in the j^{th} interval.

- All values of j^{th} interval are multiply by $SF(j)$.

4.3 Results

Fourteen channels, corresponding to ocular artifact contaminated EEG signal (10s), are selected from total 34 channels of EEG dataset [74] and these 14 channels are plotted in Fig 4.4. The x-axis shows time in seconds and the y-axis shows channel number.

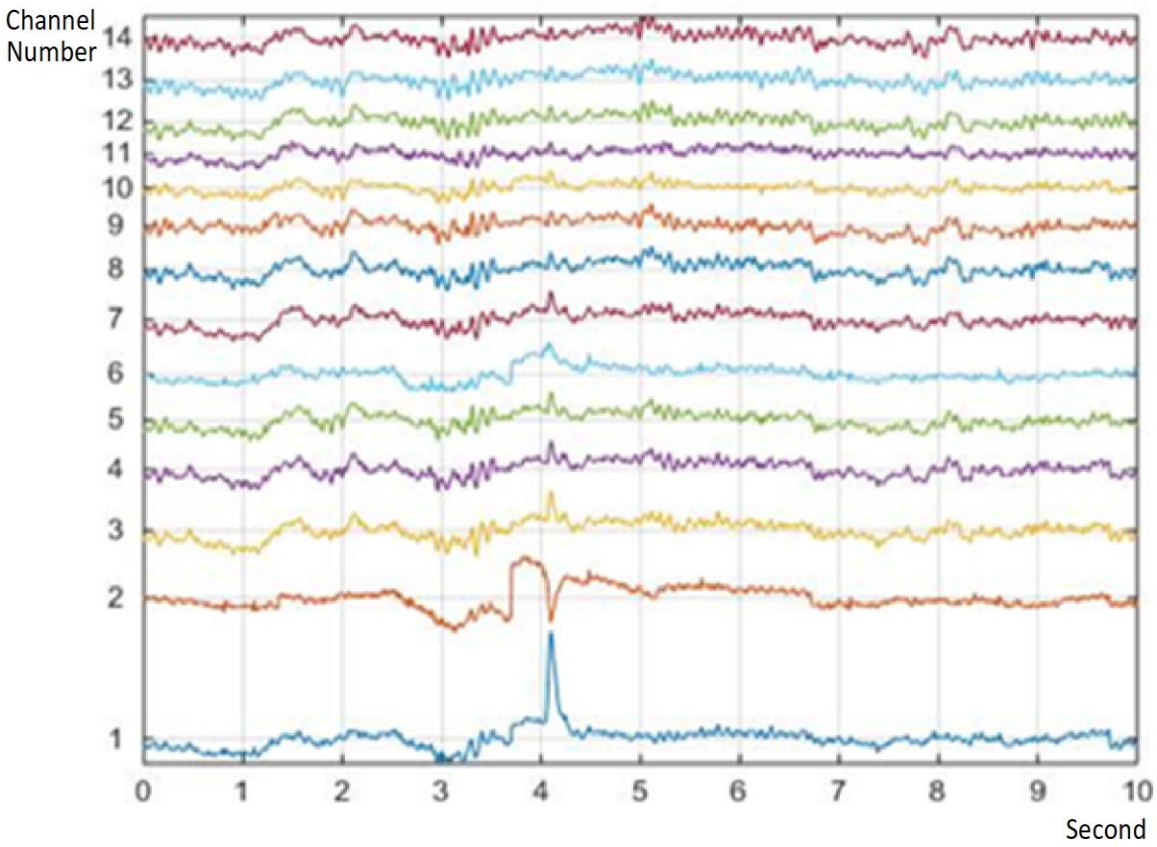

Fig 4.4: Raw (Contaminated) EEG

From Fig 4.4, it is clearly visible that channel 1 is severely affected by ocular artifact around time instant 4s. After decomposition of raw signal (correspond to all 14 channels) using Infomax ICA, 14 independent components are obtained. As per second condition of ICA decomposition, the number of recording channels is equal to the number of independent sources (or ICs). The ICs are plotted in Fig 4.5.

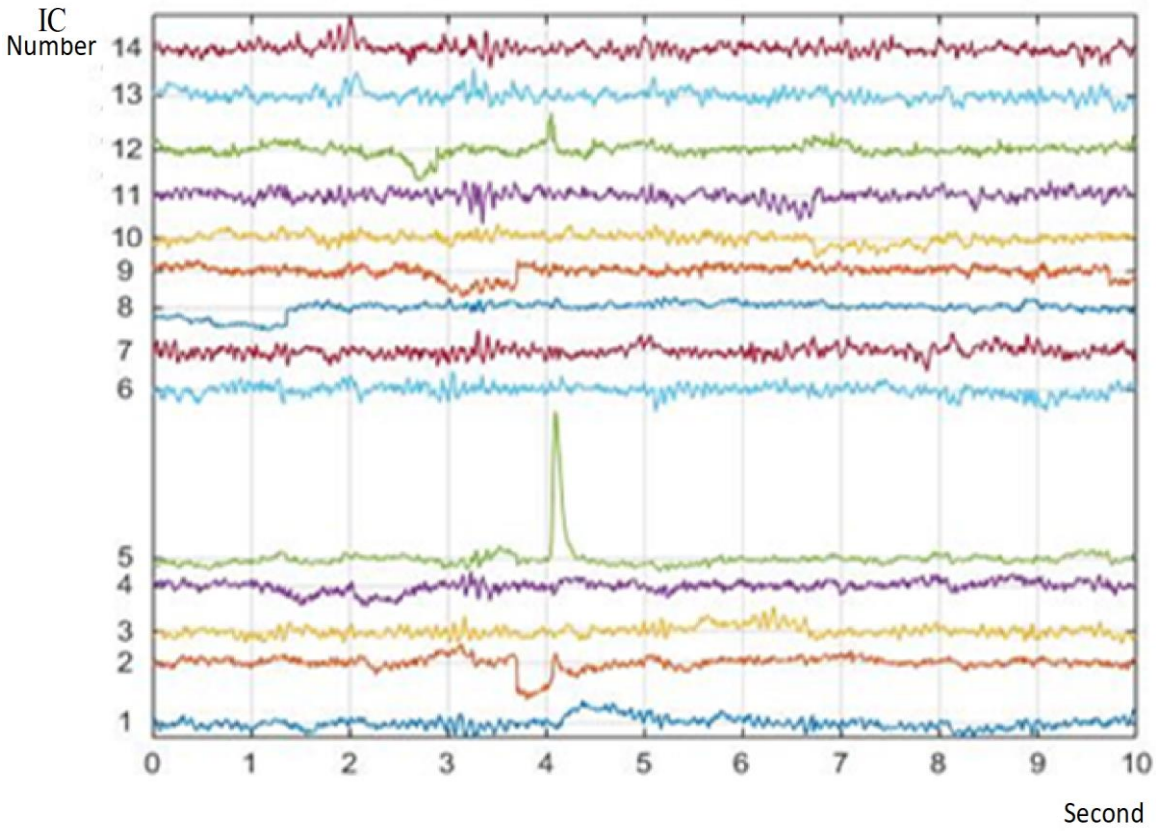

Fig 4.5: Independent components of raw EEG data (correspond to all 14 channels)

The quantities mMSE and Kurtosis for ICs of channel 1 signal are calculated and plotted as shown in Fig 4.6 and Fig 4.7 respectively. The y-axis shows sample entropy or Kurtosis for IC and the x-axis shows IC number.

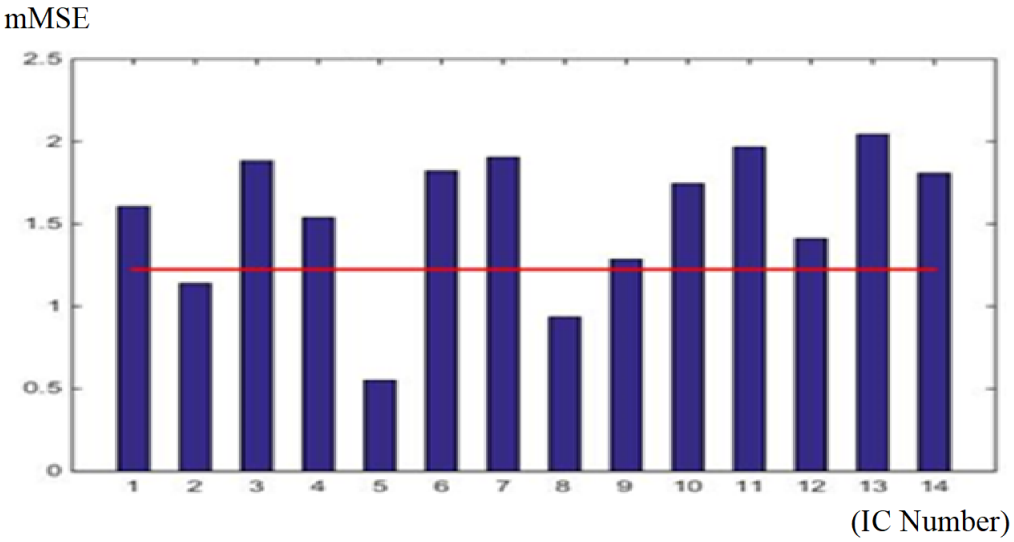

Fig 4.6: Plot of mMSE

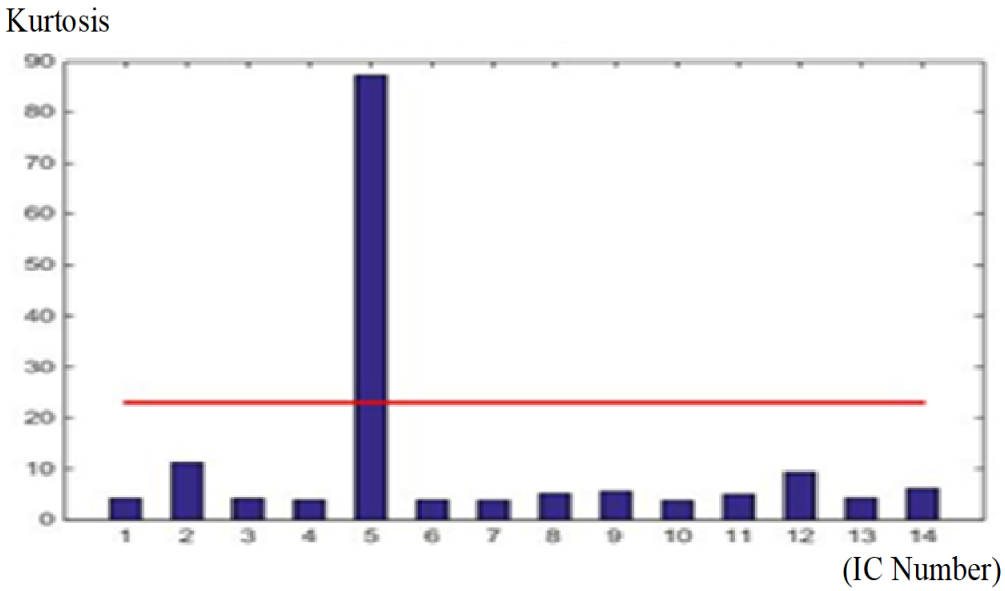

Fig 4.7: Plot of Kurtosis

The threshold value (lower limit) of mMSE and threshold value (upper limit) of Kurtosis are calculated using equations (4.7) and (4.8) respectively. The threshold value of mMSE and Kurtosis are equal to 1.26 and 22.7 respectively in this case. ICs having mMSE values less than the lower limit or Kurtosis value above upper limit are considered as artifactual components. It can be noticed from Fig 4.6 and Fig 4.7 that IC 2, 5 and 8 are affected by the ocular artifact. Then SWT and novel thresholding technique are applied to

artifactual components to suppress artifact. Finally, the artifact-free signal is reconstructed by using artifact-free ICs, artifactual ICs (after restoration) and mixing matrix of ICA. Final reconstructed artifact-free channel 1 signal is shown in Fig 4.8 with other channel signals.

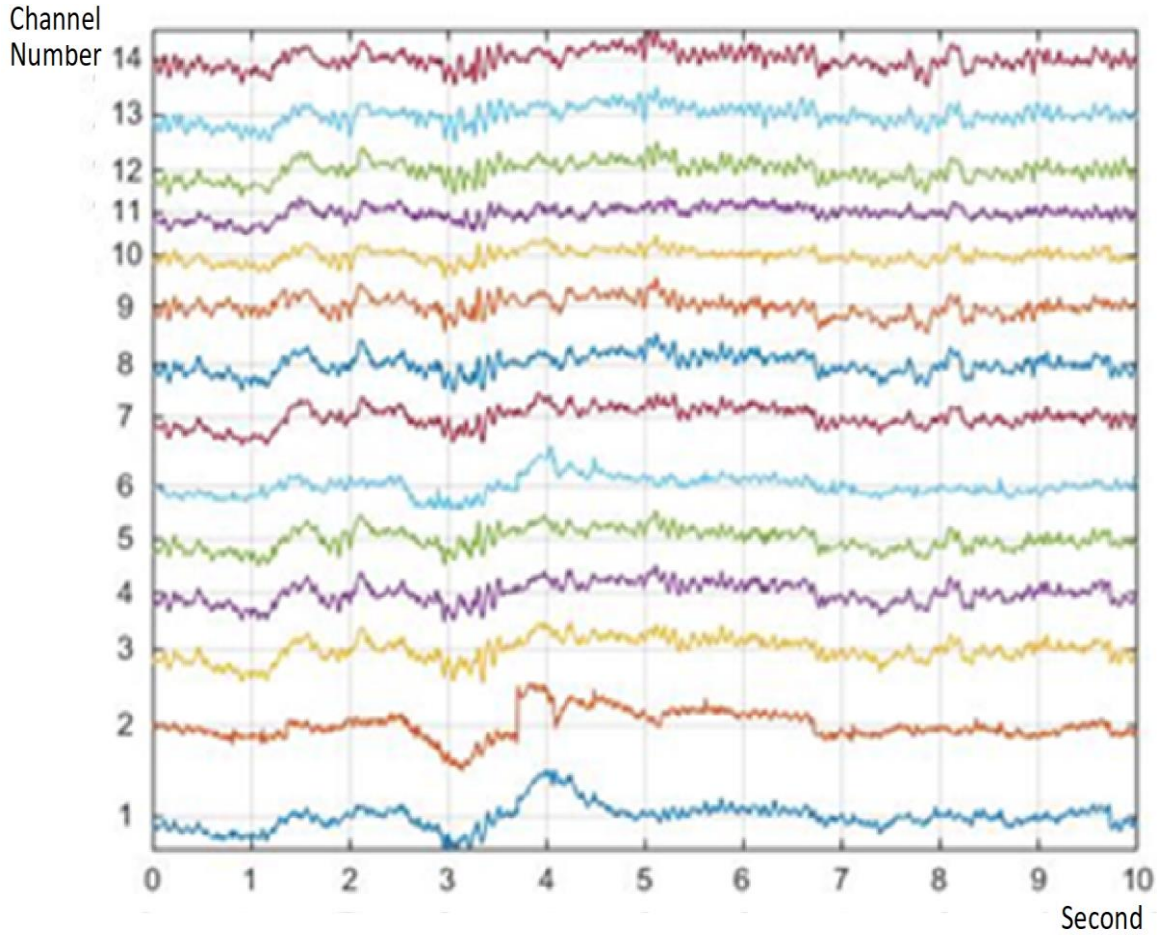

Fig 4.8: Reconstructed artifact-free signal

It can be observed from Fig 4.8 that ocular artifact has been efficiently removed from artifactual channels while keeping the rest signal unfazed. The result of proposed novel thresholding technique is compared with the result of hard thresholding. In both cases, DWT with bior-4.4 mother wavelet is used. Corresponding results are shown in Fig 4.9. In this plot, the x-axis shows the number of samples in signal and the y-axis shows EEG amplitude (μV).

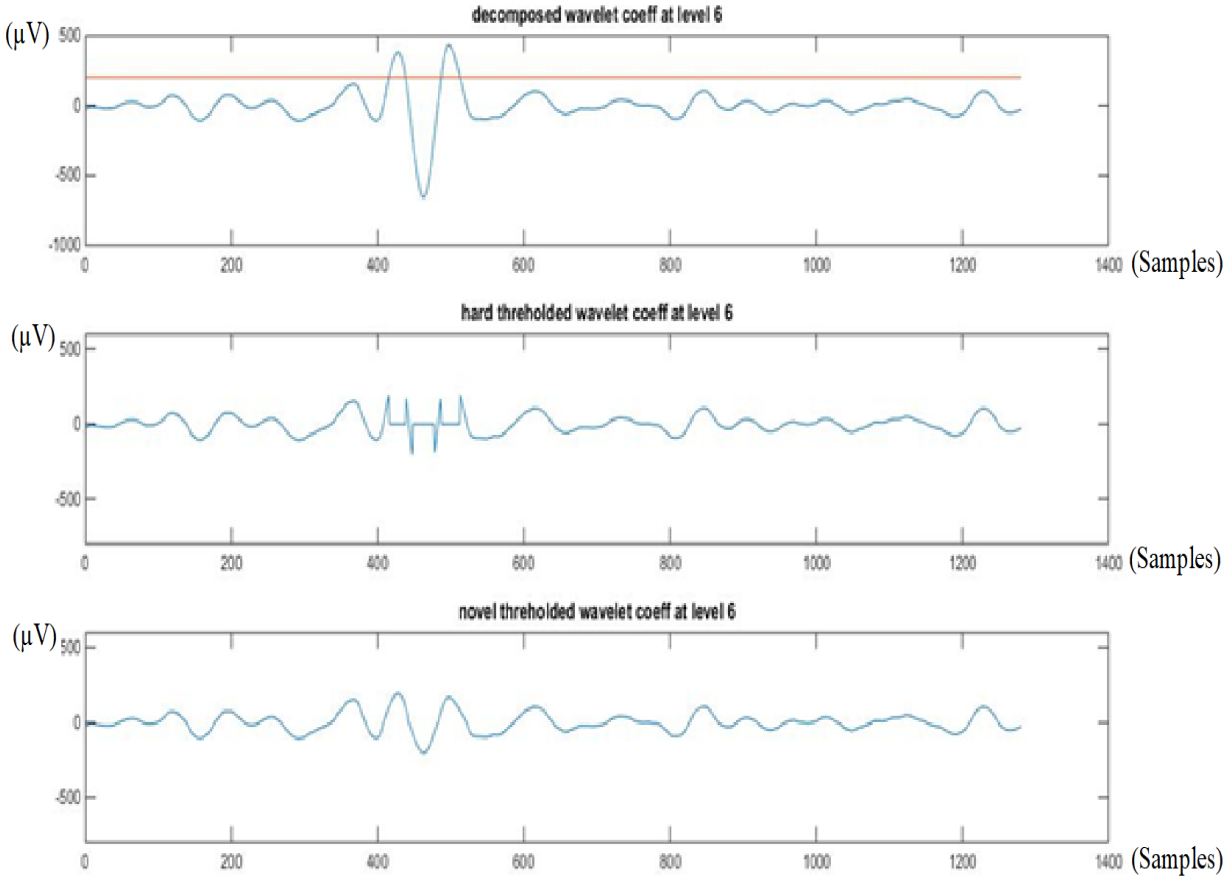

Fig 4.9: Comparison of proposed novel thresholding technique

It can be seen that hard thresholding introduce undesired discontinuities, while proposed novel thresholding technique is not only suppressing the noise part but also maintaining the smoothness of the signal.

To measure the performance of the proposed method, the results are compared with most recent techniques in terms of Correlation Coefficient, Mutual Information and Coherence for 20 different EEG signals from different datasets [74]. Correlation Coefficient is used to measure the linear relationship between two random variables [75] and it is defined as

$$r_{xs} = \frac{cov\,(x,s)}{\sigma_x\,\sigma_s} \tag{4.10}$$

where x is the raw EEG signal, s is the artifact-free EEG signal, σ_x is the standard deviation of raw EEG signal, σ_s is the standard deviation of artifact-free EEG signal and '*cov'*

is the covariance of *x* and *s*. Value of correlation coefficient lies between -1 to $+1$. A positive correlation indicates that as the values of one variable increase the values of the other variable increase, whereas a negative correlation indicates that as the values of one variable increase the values of the other variable decrease.

Mutual information (MI) of two random variables is a measure of mutual dependence between the two variables [76]. More specifically, it quantifies the amount of information obtained about one random variable, through the other random variable. If two random variables are closely related they will have large value of MI. According to Shannon information theory, MI can be calculated by Kullback-Leibler distance between the product of the marginal pdfs of random variable *x* and *y* and their joint pdf, $f\ (x, y)$. MI is defined as

$$MI\ (x, y) = \int_{-\infty}^{\infty} \int_{-\infty}^{\infty} f\ (x, y) \log \left(\frac{f\ (x,y)}{f\ (x) f(y)} \right)\ dx\ dy \qquad (4.11)$$

The marginal pdfs of random variable *x* and *y* and their joint pdf can be calculated by using either kernel density estimators or 2D-histogram. MI is always positive and there is no bound on the maximum value of MI.

Results of the proposed method are compared in terms of correlation coefficient and mutual information with latest methods. Results are shown in table 10 and table 11 respectively for 20 different EEG signals datasets with multiple channels.

Table 10: Correlation coefficient for different EEG signals

Signal Number	***Correlation Coefficient***		
	Zeroing ICA	***wICA***	***Proposed Method***
1	0.4443	0.5835	0.8606
2	0.7034	0.7936	0.9751
3	0.7809	0.8315	0.9753
4	0.8690	0.8957	0.9866
5	0.8243	0.8653	0.9870
6	0.7419	0.8150	0.9768
7	0.7889	0.8422	0.9790
8	0.9382	0.9520	0.9906
9	0.8338	0.8565	0.9971
10	0.7931	0.8487	0.9841
11	0.8682	0.8857	0.9852
12	0.8766	0.9015	0.9925
13	0.8798	0.9106	0.9960
14	0.9217	0.9371	0.9915
15	0.7432	0.9211	0.9743
16	0.8854	0.9436	0.9912
17	0.9144	0.9672	0.9935
18	0.8971	0.9554	0.9808
19	0.9085	0.9778	0.9906
20	0.8637	0.9296	0.9894

It can be observed that proposed method has the higher value of Correlation Coefficient compared to other methods for all EEG signals. The maximum value of Correlation Coefficient in case of the proposed method is 0.9991 for EEG signal 9, which is very close to the maximum possible value of Correlation Coefficient (+1).

Table 11: Mutual Information for different EEG signals

Signal Number	***Mutual Information***		
	Zeroing ICA	***wICA***	***Proposed Method***
1	0.3043	0.4213	0.6093
2	0.4967	0.6191	0.8159
3	0.4991	0.6241	0.9568
4	0.6915	0.7022	0.9784
5	0.6407	0.7315	1.0551
6	0.5815	0.6057	1.1179
7	0.6008	0.7123	0.9953
8	0.9769	1.1989	1.6181
9	0.6134	0.9528	1.5221
10	0.5712	0.7498	1.0794
11	0.7344	0.8187	1.7097
12	0.7245	0.9009	1.6661
13	0.8090	0.9772	1.6155
14	0.9765	1.2705	1.5738
15	0.8573	1.1822	1.4896
16	0.7855	0.9781	1.4027
17	0.9468	1.2062	1.6023
18	0.9211	1.1843	1.5971
19	0.8855	1.1642	1.4428
20	0.9062	1.1267	1.5115

It can be observed that for all EEG signals, the proposed method has the higher value of MI compared to other methods. The maximum value of MI for the proposed method is 1.7097 for EEG signal 11.

To analyze the performance in the frequency domain, Coherence is measured between raw EEG data and artifact-free EEG data. Coherence measures the degree of linear dependency of two signals by testing for similar frequency components. Coherence function is defined as

$$C_{xs}(\omega) = \frac{P_{xs}(\omega)}{\sqrt{P_{xx}(\omega)P_{ss}(\omega)}} \tag{4.12}$$

where $P_{xx}(\omega)$ is the power spectra of raw EEG signal, $P_{ss}(\omega)$ is the power spectra of artifact-free EEG signal signals, $P_{xs}(\omega)$ is the cross-power spectrum for these signals and ω is frequency.

If two signals match each other perfectly at a given frequency, the magnitude of coherence function is 1. If they are totally unrelated, the value of Coherence function will be 0. Coherence is plotted in Fig 4.10- 4.12 for channel-1signal of raw EEG signal of Fig.4.4 and channel-1 signal of artifact-free EEG signal of Fig.4.8. In these plots, the x-axis shows the frequency and the y-axis shows the amplitude of Coherence function.

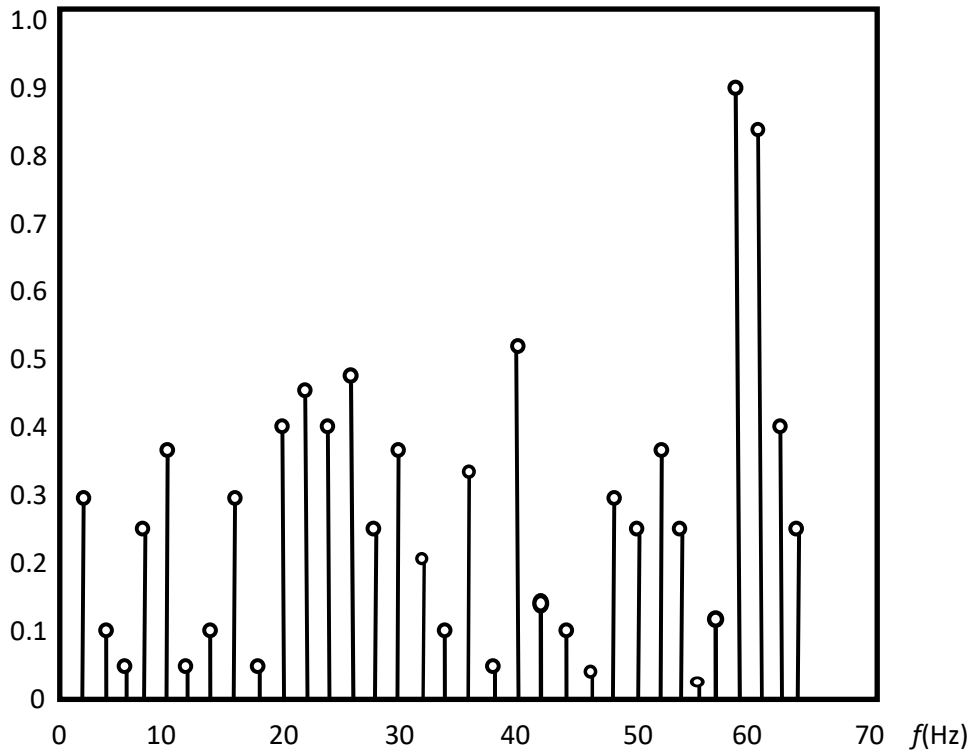

Fig 4.10: Coherence of zeroing ICA

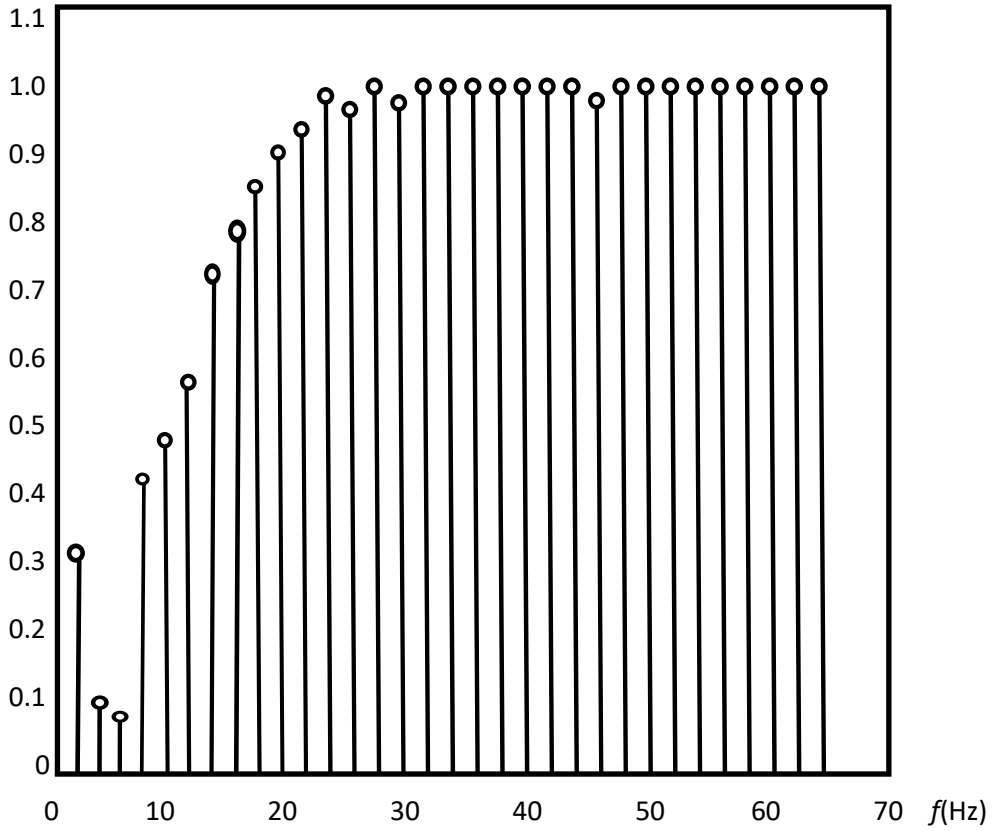

Fig 4.12: Coherence of wICA

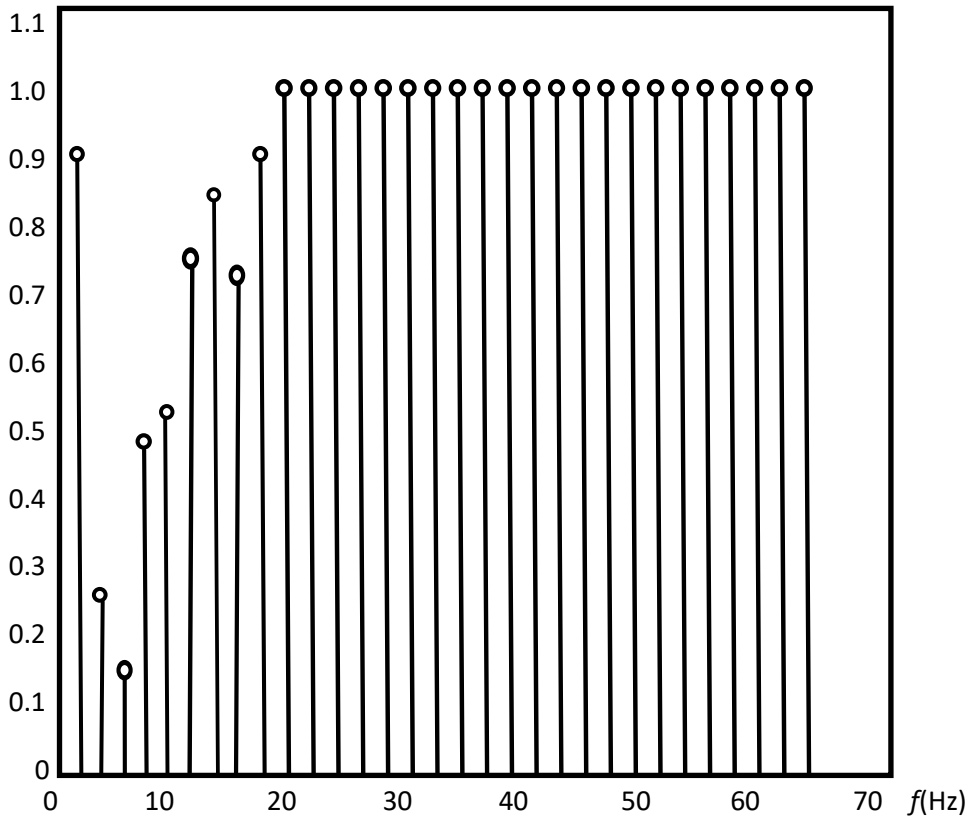

Fig 4.12: Coherence of proposed method

It can be observed that value of Coherence function is less for lower frequency components than higher frequency components for all methods. It verifies that lower frequency components are more affected by ocular artifact than higher frequency components. The proposed method results in higher values of Coherence function for artifact affected lower frequency components and almost constant (approximately equal to 1) value of Coherence function for higher frequency components. These two facts prove the superiority of the proposed method over other methods.

4.4 Significant Findings

The proposed method effectively removes the ocular artifact from EEG signal and properly retains morphological information present in the EEG signal by using SWT and proposed thresholding technique respectively. SWT improves denoising capability and morphological information retaining capability by handling shift variance and aliasing issues of DWT. Proposed novel thresholding technique further enhances morphological information retaining capability by properly handling discontinuities issues in case of other thresholding techniques.

This chapter is based on the following work:

Mahipal Singh Choudhry, Rajiv Kapoor "*Ocular Artifact Removal from EEG using Stationary Wavelet Enhanced ICA*", International Journal of Control Theory and Applications (**ISSN:** 0974-5572, Scopus index journal with SJR: 0.53), 2016, vol: 9, no: 10, pp: 4935-4945 [68]. .

CHAPTER 5

A NEW METHOD FOR MR IMAGE SEGMENTATION

This chapter includes the details of the local region based energy function, two-phase level set formulation, multi-phase level set formulation, equation updating, proposed methodology, results and comparative analysis of results.

5.1 Introduction

A novel fuzzy energy based level set method [77] is proposed for MR image segmentation. A new region-based level set model with FCM based energy function and Distance Regularized Level Set Evolution (DRLSE) is proposed to deal with noise and intensity inhomogeneity in the medical image. In this method, FCM based energy function is used to overcome the local minimum problem of active contour modal and DRLSE is used to deal with the re-initialization problem of traditional level set method. These two modifications in level set modal effectively deals with intensity inhomogeneity of medical image. A Mean filter like spatial term is also utilized with the proposed FCM based energy function, which makes this method advantageous for segmenting noisy medical images.

5.2 Proposed Methodology

The workflow diagram of the proposed framework is depicted in Fig 5.1.

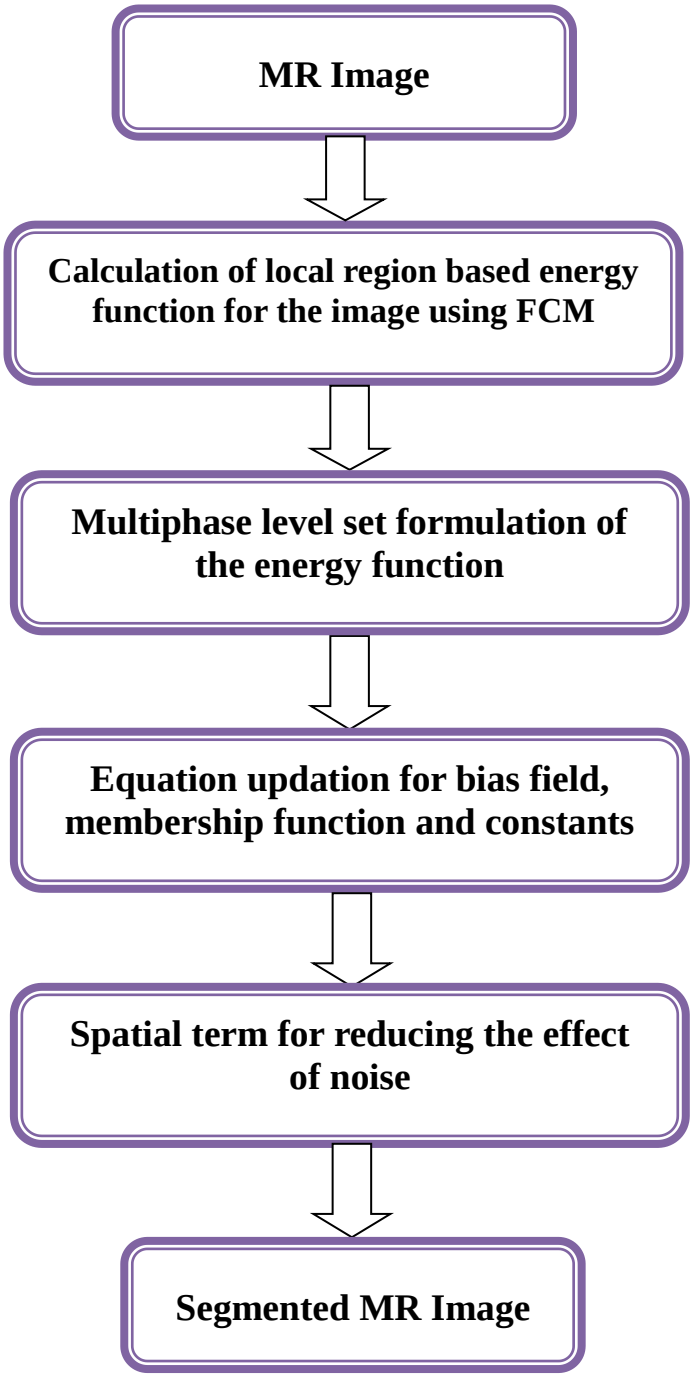

Fig 5.1: Flowchart of the proposed method for MR image segmentation

The proposed method is implemented using following steps: -

- Calculation of the local region based energy function for image by using the FCM.
- Multi-phase level set formulation.
- Equations updation.
- Spatial term for reducing noise effect.

In proposed research work, the median filter is used as preprocessing step for edge-preserving smoothing of medical images.

5.2.1 Local Region Based Energy Function using FCM

The local region based model is used to define energy function of proposed model by using the FCM concept. Each pixel is assigned to a particular region of the image, based on its membership function. For the medical image, this arrangement of pixel assignment is more suitable instead of hard assignment and this membership function is also utilized to reduce the effect of noise [78]. This energy function is FCM objective function of partitioning a dataset $\{x_1,\ x_2, \ldots\ldots\ldots\ldots x_M\}$ into N clusters and it is given by

$$J_m = \sum_{i=1}^{N} \sum_{k=1}^{M} u_{ik}^{m}(x) \, \|x_k - v_i\|^2 \tag{5.1a}$$

where $\|\quad\|$ stand for the Euclidean norm, v_i is the centroid of the i^{th} cluster, u_{ik} is membership function and m is the fuzzy factor. There are two purposes to be achieved using energy function, one is segmentation of image and other is to estimate the bias field.

Real world images can be represented as a multiplicative field, added by noise [89]. This can be written as

$$I = bJ + n \tag{5.1b}$$

where I is observed image, J is the true image, b represents bias field term, which represents intensity inhomogeneity and n is the additive Gaussian noise with zero mean and

constant variance. It is the most common type of noise in medical images results from the contributions of many independent signals.

The assumptions made in this model are: -

- The true image J is assumed as a piecewise constant i.e. in a given region Ω_i, it takes a constant value c_i.
- Bias field b varying very slowly, which implies that in a small neighborhood, b is constant.

Value of bias field, in a local neighborhood region, is considered constant for given image [79], i.e., for a circular region O_y of the image (shown in Fig 5.2), value of the bias field is

$$b(x) \approx b(y) \qquad \text{for} \qquad x \in O_y \tag{5.2}$$

where, $O_y \subset \{x: |x - y| \leq r\}$, r represents the radius of circular region O_y, y is the center of O_y and $y \in \Omega$ (image domain).

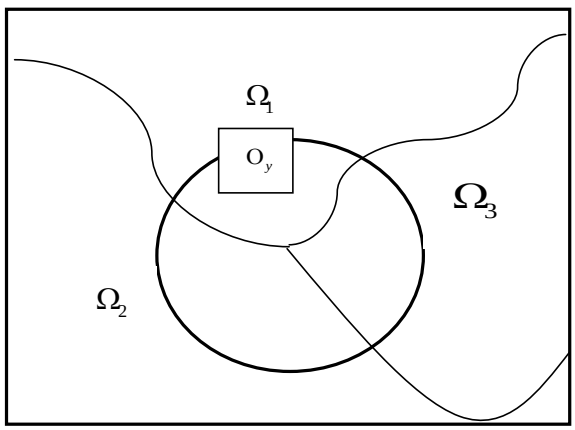

Fig 5.2: Representation of local region O y

By using equations 5.1 and 5.2, the intensity in the local region is written as

$$I(x) = b(y)J(x) + n(x) \qquad \text{for} \qquad x \in O_y \tag{5.3}$$

By using the first postulation about *J*(*x*), ***I(x)*** given by equation 5.3 is rewritten as

$$I(x) = b(y)c_i + n(x) \qquad \text{for} \qquad x \in O_y \cap \Omega_i \tag{5.4}$$

The additive Gaussian noise term can be eliminated if pixels (in a region, Ω_i) are considered to be part of a Gaussian distribution with mean $m_i = b(y)c_i$. The local region O_y can be divided into N clusters, having centers at $m_i \approx b(y)c_i$, i vary from 1 to N.

The energy term of the local region is calculated using the FCM concept with the Chan-Vese piece-wise constant model of the image and it is given by

$$F_y = \sum_{i=1}^{N} \int_{O_y \cap \Omega_i} u_i^m(x)\,(I(x) - m_i)^2 dx \tag{5.5}$$

where u_i and m are membership function and fuzzy factor respectively. The fuzzy factor m decides the fuzziness and normally it is taken as 2. In a local region, O_y, the center of the cluster m_i can be replaced by $b(y)c_i$ and a window function [79]. The window function is characterized as

$$W(y - x) = 0, x \notin O_y \tag{5.6}$$

By using equations 5.5 and 5.6, energy can be written in term of window function as

$$F_y = \sum_{i=1}^{N} \int_{\Omega_i} u_i^m(x) W(y - x)\,(I - b(y)c_i)^2 dx \tag{5.7}$$

The overall energy for total image domain (Ω) is given by

$$F(b, c, u, \Omega_1, \Omega_2 \ldots \Omega_N) \triangleq \int \left\{ \sum_{i=1}^{N} \int_{\Omega_i} u_i^m(x) W(y - x)\,(I - b(y)c_i)^2 dx \right\} dy \tag{5.8}$$

where, c= $\{c_1, c_2 \ldots . c_N\}$ represents the constants.

The selection of window function is flexible. It should take null values outside the local region for a given x and y. *W (z)* = 0 for $|z| > r$ and inside the region, it should have a sum of unity i.e. $\int W(z) = 1$ [80]. *W (z)* used in this model is

$$W(z) = \begin{cases} \frac{1}{a}\, e^{-|z|^2/2\sigma^2} & \text{for } |z| \le r \\ 0 & \text{otherwise} \end{cases} \tag{5.9}$$

Selection of the parameter a depends on the value of σ (standard deviation) such that relation $\int W(z) = 1$ is satisfied. The selection of r is one of the crucial factors and the assumptions made on bias field are valid only when the neighbourhood is small. The bias field varies faster so the value of r should be small.

5.2.2 Level Set Formulation

Level set formulation for the biomedical image is first implemented for two-phase and then for multi-phase. The concept of distance regularized level set evolution (DRLSE) [55] is used to deal with the re-initialization problem of the level set model.

5.2.2.1 Two-Phase Level Set Formulation

In two-phase level set model contour/curve, C is represented by zero level set of the level set function $\phi\ (x)$ and the image is divided into two regions Ω_1 and Ω_2 using a single level set function $\phi\ (x)$.

In the proposed model, the two regions are defined using the level sets $M_1(\phi)$ and $M_2(\phi)$ [81]. $M_1(\phi)$ and $M_2(\phi)$ are given as

i. Level set in the region $\boldsymbol{\Omega_1}$, $\boldsymbol{M_1(\phi) = H(\phi)}$

ii. Level set in the region Ω_2, $M_2(\phi) = \{1 - H(\phi)\}$

where $H(\phi)$ represents Heaviside function and it is defined as

$$H(z) = \begin{cases} 1 & \text{if } z \geq 0 \\ 0 & \text{if } z < 0 \end{cases}$$

The energy function is modified using these definitions and equation 5.8 as

$$F(b, c, u, \phi) \triangleq \int \left\{ \sum_{i=1}^{2} \int u_i^m\ (x) W(y - x)\ (I - b(y) c_i)^2 M_i\big(\phi(x)\big) dx \right\} dy \quad (5.10)$$

By exchanging the order of integration, equation 5.10 becomes

$$F(b, c, u, \phi)\ \triangleq \int \sum_{i=1}^{2} u_i^m\ (x)\ e_i(x)\ M_i\big(\phi(x)\big) dx \quad (5.11)$$

where $e_i(x)$ is defined as

$$e_i(x) = \int W(y-x)\,(I - b(y)c_i)^2 dy \tag{5.12}$$

The quantity $e_i(x)$ is rearranged as

$$e_i(x) = I^2 1_K - 2c_i I(b * W) + c_i^2(b^2 * W) \tag{5.13}$$

where $*$ represents the convolution and

$$1_K = \int W(y-x)dy \tag{5.14}$$

As per Chan-Vese model, energy function for the level set form is given by adding regularizing terms to the fitting energy [89] as

$$F_{cv}(b,c,u,\phi) = F(b,c,u,\phi) + v\,L(\phi) + \mu\,R_p(\phi) \tag{5.15}$$

In this equation, $F(b,c,u,\phi)$ is used as data term. $L(\phi)$ and $R_p(\phi)$ act as regularizing terms [89] and are defined as

$$L(\phi) = \text{Length}\,(C) = \text{Length}\,(\phi = 0) = \int_\Omega |\nabla H(\phi)| dx = \int_\Omega \delta_o(\phi)|\nabla\phi| dx \tag{5.16}$$

and

$$R_p(\phi) = \text{Area}\,(\Omega_1) = \text{Area}\,(\phi \geq 0) = \int_\Omega H(\phi)dx \tag{5.17}$$

where μ and v are constant parameters. δ_o represents Dirac delta function and given as

$$\delta_o(z) = \frac{d\,H(z)}{dz}$$

where $L(\phi)$ represents the length of contour (or zero level set) and serves the purpose of keeping the curve smooth by regularizing the contour. The term $R_p(\phi)$ is used to avoid re-initialization in level set evolution[80].

5.2.2.2 Distance Regularized Level Set Evolution (DRLSE)

Re-initialization is one of the disadvantages of the traditional level set model. During level set evolution, they develop irregularities and leads to errors. To overcome this, formal approach is to stop the evolution by using a signed distance function to redesign it. It is quite tricky to predict suitable time to apply re-initialization. To overcome this conflict,

Li et al planned a term, called as distance regularized level set evolution (DRLSE) [55]. In level set functions, signed distance is maintained by DRLSE and gradient descent, for the evolution of level set function, is specified as

$$\frac{\partial \phi}{\partial t} = -\frac{\partial F_{cv}}{\partial \phi} \tag{5.18}$$

When energy term $F_{cv}(b, c, u, \phi)$ is minimized with reference to ϕ (b, c as constants), equation 5.18 result in

$$\frac{\partial \phi}{\partial t} = \delta(\phi)\left\{(u_1^m e_1 - u_2^m e_2) + v\, div\left(\frac{\nabla \phi}{|\nabla \phi|}\right)\right\} + \mu\, div\{d_p(|\nabla \phi|)\nabla \phi\} \tag{5.19}$$

where $$d_p(z) \triangleq \frac{p(s)}{s} \tag{5.20}$$

To achieve optimal solution using energy function along with level sets function, values of bias field b and constants c are also updated in a repetitive manner.

5.2.2.3 Multi-Phase Level Set Formulation

The two-phase model can be extended to multiphase model [83] for image segmentation using proposed energy function. In this case, k ≥ $\log_2$ N level sets are required to solve the N-phase problem. Ω can be divided into N regions, which are represented by $M_i\{\phi_1(x), \phi_2(x) \dots \dots \dots \phi_k(x)\}$ and are defined as

$$M_i\{\phi_1(x), \phi_2(x) \dots \dots \dots \phi_k(x)\} = \begin{cases} 1, & \text{if } x \in \Omega_i \\ 0, & \text{otherwise} \end{cases} \tag{5.21}$$

where, $\boldsymbol{\phi} = \{\phi_1, \phi_2 \dots \dots \dots \phi_k\}$ represent the level set vector.

Energy function for multiphase is written as

$$F(b, c, u, \boldsymbol{\phi}) \triangleq \int \sum_{i=1}^{N} u_i^m(x)\, e_i(x)\, M_i\big(\phi(x)\big)dx \tag{5.22}$$

Chan-Vese energy function for level set form is given by adding regularizing terms to the fitting energy as

$$F_{cv}(b, c, u, \boldsymbol{\phi}) = F(b, c, u, \boldsymbol{\phi}) + v\sum_{j=1}^{k} L\big(\phi_j\big) + \mu\sum_{j=1}^{k} R_p(\phi_j) \tag{5.23}$$

The gradient descent equations are obtained in similar way to two phase set and they are obtained by minimizing $F_{cv}(b, c, u, \boldsymbol{\phi})$ with respect to $\boldsymbol{\phi}$ (b, c as constants) as

$$\frac{\partial \phi_j}{\partial t} = \sum_{i=1}^{N} \frac{\partial M_i(\phi)}{\partial \phi_j} u_i^m(x) e_i(x) + \delta(\phi_j)\, v\, div\left\{\frac{\nabla \phi_j}{|\nabla \phi_j|}\right\} + \mu\, div\{d_p(|\nabla \phi_j|)\nabla \phi_j\} \qquad (5.24)$$

where j = 1, 2……k.

5.2.3 Equation Updation

The updating equations for the bias field b, membership function u and constants c are obtained by minimizing $F_{cv}(b, c, u, \boldsymbol{\phi})$ with respect to b, u or c and by keeping other variables constant.

5.2.3.1 Equation Updation for Constants

To get the update equation for constants, $F_{cv}(b, c, u, \boldsymbol{\phi})$ is minimized with reference to c by keeping b, u and ϕ as constants. For derivative of $F_{cv}(b, c, u, \boldsymbol{\phi})$ with respect to c_j by taking b, u and ϕ as constant, all other terms of the summation in equation 5.23 are independent of c_j , except the j^{th} term so by putting derivative of $F_{cv}(b, c, u, \boldsymbol{\phi})$ equal to zero, following relation is obtained

$$\frac{\partial F_{cv}(b,c,u,\phi)}{\partial c_j} = \int u_j^m(x) \frac{\partial e_j(x)}{\partial c_j} M_j(\phi) dx = 0 \qquad (5.25)$$

Derivative of $e_i(x)$ with respect to c_j (by taking b, u and ϕ as constant) is

$$\frac{\partial e_j(x)}{\partial c_j} = -2 \int W(y - x)\, (I - b(y)\widehat{c_j}) b(y) \qquad (5.26)$$

By using equations 5.25 and 5.26

$$\frac{\partial F_{cv}(b,c,u,\phi)}{\partial c_j} = \int u_j^m(x) \int W(y - x)\big(I(x) - b(y)\widehat{c_j}\big)\, b(y) M_j(\phi) dx = 0 \qquad (5.27)$$

$$\int u_j^m(x) I(x) M_j(\phi) \left(\int W(y - x) b(y) dy\right) dx =$$

$$\widehat{c_j} \int u_j^m(x) M_j(\phi) \left(\int W(y - x) b^2(y) dy\right) dx \qquad (5.28)$$

Hence $$\widehat{c_j} = \frac{\int (b*W) IM_j(\phi) dx}{\int (b*W) M_j(\phi) dx} \quad (5.29)$$

where $j = 1, 2 \ldots . . N$

5.2.3.2 Equation Updation for Bias Field

Equation for bias field is updated by minimizing $F_{cv}(b, c, u, \boldsymbol{\phi})$ with respect to b by keeping c, u and ϕ as constants. To minimize $F_{cv}(b, c, u, \boldsymbol{\phi})$ derivative of $F_{cv}(b, c, u, \boldsymbol{\phi})$ with respect to b is set equal to zero, which result in following relation

$$\frac{\partial F_{cv}(b,c,u,\boldsymbol{\phi})}{\partial b(y)} = \sum_{i=1}^{N} \int u_i^m(x) \frac{\partial e_i(x)}{\partial b} M_i(\phi) dx = 0 \quad (5.30)$$

Derivative of $e_i(x)$ with respect to b (by taking c, u and ϕ as constant) is

$$\frac{\partial e_i(x)}{\partial b(y)} = -2W(y-x)\big(I(x) - \hat{b} c_i\big) c_i \quad (5.31)$$

By using equations 5.30 and 5.31

$$\frac{\partial F_{cv}(b\ ,c,u,\Phi)}{\partial b(y)} = \sum_{i=1}^{N} u_i^m(x) W(y-x)\big(I(x) - \hat{b}\ c_i\big) c_i\ M_i(\Phi) dx = 0 \quad (5.32)$$

Hence

$$\int W(y-x) \{\sum_{i=1}^{N} u_i^m I(x) M_i(\Phi) c_i\}\, dx = \hat{b} \{\int W(y-x) (\sum_{i=1}^{N} u_i^m M_i(\Phi) c_i^2) dx\} \quad (5.33)$$

$$\hat{b} = \frac{(I\ J^{(1)}) * W}{(J^{(2)}) * W} \quad (5.34)$$

where $$J^{(1)} = \sum_{i=1}^{N} M_i(\Phi) c_i u_i^m \quad (5.35)$$

$$J^{(2)} = \sum_{i=1}^{N} M_i(\Phi) c_i^2 u_i^m \quad (5.36)$$

5.2.3.3 Equation Updation for Membership Function

To get updating equation for membership function, energy term is solved using Lagrange multiplier as

$$F_m = F_{cv} + \lambda\{1 - \sum_{i=1}^{k} u_i^m(x)\} \quad (5.37)$$

and $$\sum_{i=1}^{k} u_i^m(x) = 1 \,, \forall\, x \tag{5.38}$$

These equations are updated by considering derivative of F_m with reference to u_j (with c, b and ϕ as constants) and equating it to zero. The estimated value of u_j is

$$\hat{u}_j = \left[\lambda / \left\{ m u_j^{m-1}(x) e_j(x) \right\}\right]^{\frac{1}{m-1}} \tag{5.39}$$

By using equations 5.38 and 5.39

$$\sum_{i=1}^{k} [\lambda / \{ m u_i^{m-1}(x)\, e_i(x) \}]^{m/(m-1)} = 1 \tag{5.40}$$

$$\lambda = [\sum_{i=1}^{k} \{ m u_i^{m-1}(x) e_i(x) \}^{-1/(m-1)}]^{-(m-1)} \tag{5.41}$$

By substituting value of λ in equation 5.39, gives

$$\hat{u}_j = \frac{\{u_j^{m-1}(x) e_j(x)\}^{-1/(m-1)}}{\sum_{i=1}^{k} \{u_i^{m-1}(x) e_i(x)\}^{-1/(m-1)}} \tag{5.42}$$

5.2.4 Spatial Term for Reducing Noise Effect

A spatial term, for fuzzy clustering using membership function, is used in the level set formulation of the proposed method to subjugate noise effect. At every step, the spatial term is also calculated along with bias filed, constants and membership function. In the proposed method, the spatial term is average of membership values of neighboring pixels and given as

$$h_i(x) = \sum_{x_r \in N_R(x)} u_i(x_r) \tag{5.43}$$

where, $N_R(x)$ represents set of all neighboring pixels.

It is like mean filter [84] applied on membership function. By taking this extra spatial term into consideration, a pixel membership value is decided by the neighboring pixels. i.e., even if the center pixel is noisy its effect can be truncated. Using this spatial term, the membership function is updated as

$$u_i(x) = \frac{u_i^p(x) h_i^q(x)}{\sum_{j=1}^{k} u_j^p(x) h_j^q(x)} \tag{5.44}$$

where p and q represent the weight given to each term. If noisy is profound, more weight is given to the spatial term by considering large values for q.

5.3 Results

The proposed method is verified for numerous synthetic images as well as real medical images and corresponding results are compared with some latest methods. Fig 5.3 displays corresponding results for evaluation of proposed method on an image of the heart.

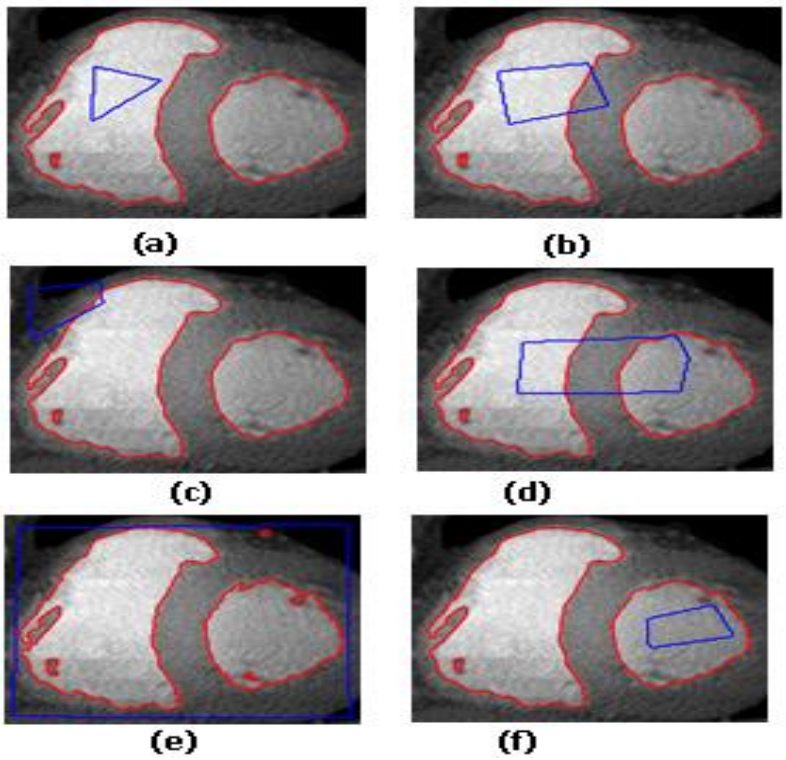

Fig 5.3: Contour evaluation using different types of initialization

Initial contour in Fig 5.3 (a) and Fig 5.3 (f) is inside of the region of interest and in Fig 5.3 (e), it is completely outside of the region. In all case, the final contour is same and results are independent of initialization of initial contour. In Fig 5.4 – 5.6, MRI images obtained from web datasets [85] [86] are used. A synthesis image, added with Gaussian

noise density (σ) of 0.02 is used to compare suggested method with other methods and corresponding outcomes are publicized in Fig 5.7.

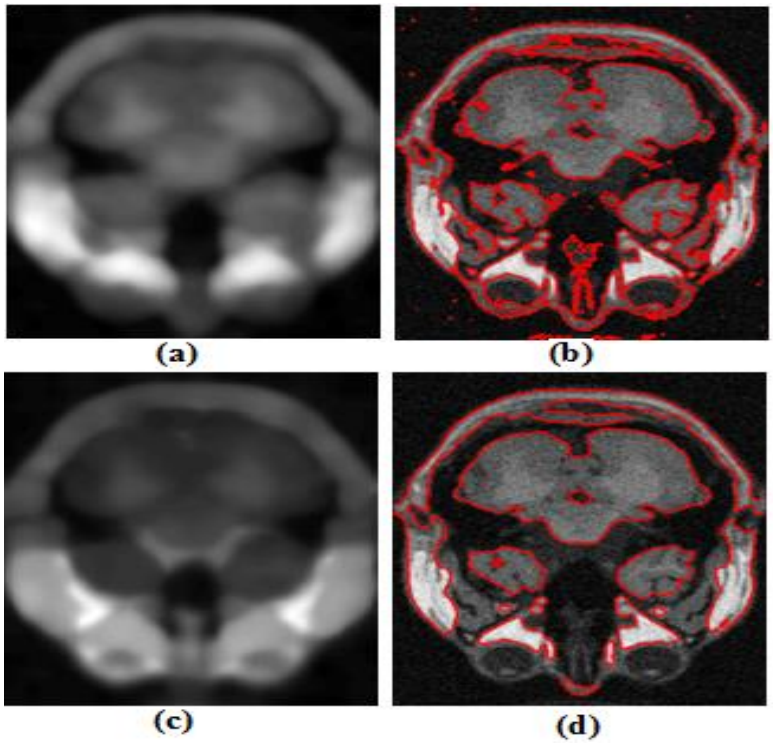

Fig 5.4: On a noisy MRI image (a, b) Bias field & final contour using C. Li et al method (c, d) Bias field & final contour using proposed method

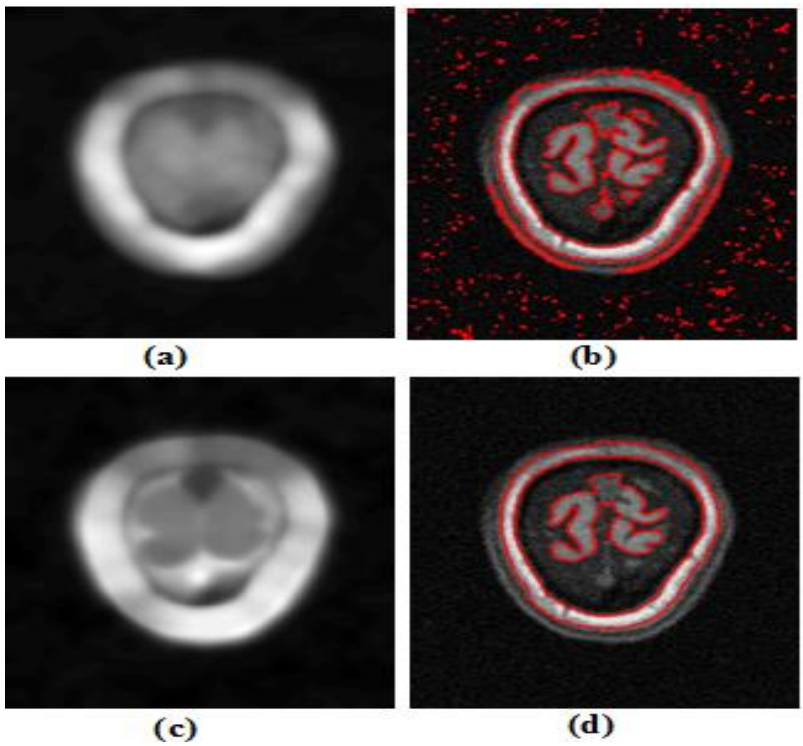

Fig 5.5: On a noisy MRI image (a, b) Bias field & final contour using B. N. Li et al method (c, d) Bias field & final contour using proposed method

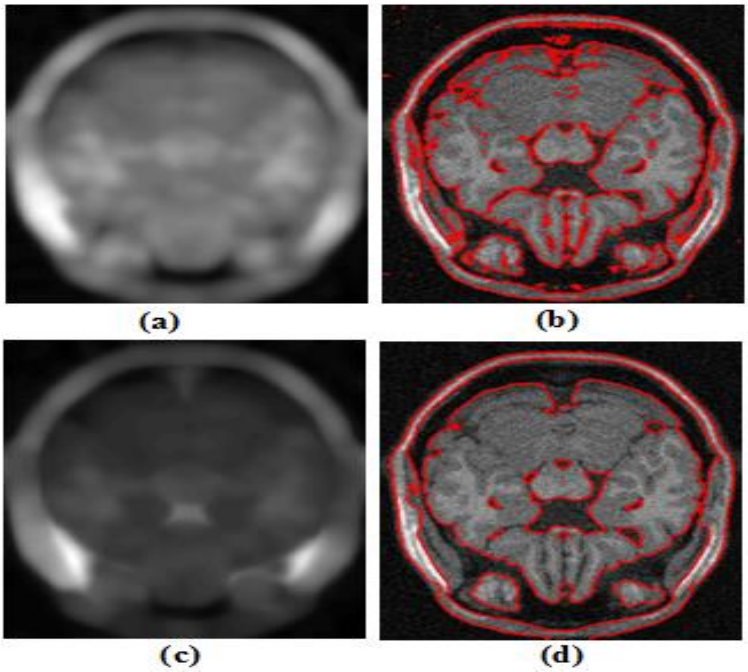

Fig 5.6: On a noisy MRI image (a, b) Bias field & final contour using W. Cui et al method (c, d) Bias field & final contour using the proposed method

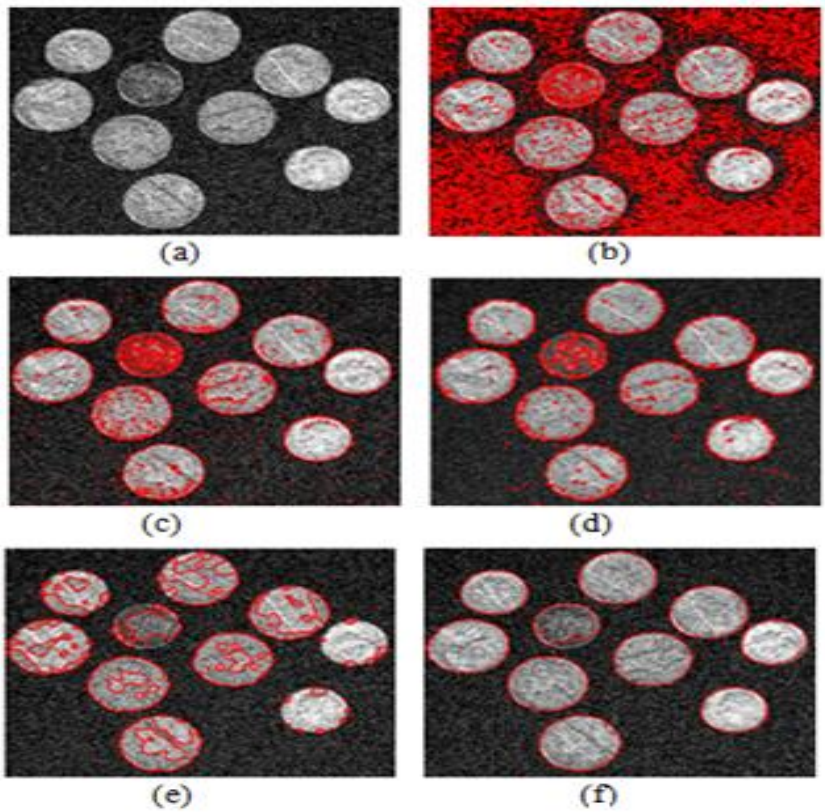

Fig 5.7 (a) Noisy image with Gaussian noise density of σ = 0.02. Results using (b) C. Li et al method (c) W. Cui et al method (d) Y. Chen et al method (e) B.N. Li et al method (f) Proposed method

Results show that final contour obtained by other methods is affected by the noise and in case of the proposed method, the noise effect is very less. The proposed method is compared with other latest methods on the basis of Segmentation Accuracy (SA) for same synthetic image corrupted by different Gaussian noise (noise density,$\sigma = 0\ to\ 0.1$). The values obtained by experimental evaluation are shown in Table 12. SA is defined as [87]

$$\text{SA} = \frac{\text{Number of Correctly Classified Pixels}}{\text{Total Number of Pixels}} \tag{5.47}$$

Table 12: **Segmentation Accuracy (SA) for Synthetic Image Corrupted by Gaussian Noise**

Method	***Noise Density***					
	0	0.02	0.04	0.06	0.08	0.10
C. Li *et al*	92.81	88.26	86.18	83.65	78.95	76.56
W. Cui *et al*	95.64	92.44	89.92	88.06	85.22	82.47
Y. Chen *et al*	92.78	89.57	85.32	82.48	78.12	77.21
B.N. Li *et al*	96.42	93.30	88.74	86.15	84.74	85.13
Proposed Method	99.85	98.23	96.28	94.76	93.42	92.38

5.4 Significant Finding

Proposed novel fuzzy energy based level set method for biomedical image segmentation not only improves segmentation accuracy but also ensure that contour evaluation is independent of initialization of initial contour. Mean filter based spatial term further improve segmentation by reducing noise effect.

This chapter is based on the following work:

Mahipal Singh Choudhry, Rajiv Kapoor "*Performance Analysis of Fuzzy C-Means Clustering Methods for MRI Image Segmentation*", Procedia Computer Science Journal (Pub: Elsevier), 2016, vol. 89, pp: 749-756 [88].

Mahipal Singh Choudhry, Rajiv Kapoor "*A Novel Fuzzy Energy Based Level Set Method for Medical Image Segmentation*", Cogent Engineering (Pub: Cogent OA, Taylor & Francis), 2018 [77].

CHAPTER 6

CONCLUSIONS & FUTURE SCOPE

This chapter highlights the conclusions drawn from this study on the basis of the contributions made either theoretically or experimentally and the details of future research directions.

6.1 Conclusions

The two new methods are proposed for artifact removal from important 1-D biomedical signals (ECG and EEG). A new method for image segmentation is proposed for most important 2-D biomedical signal, MRI. These methods are as follows:

- In the first method a cascade combination of Complete Ensemble Empirical Mode Decomposition (CEEMD) and morphological functions using adaptive structuring elements (SE), is used for baseline wander removal from the important 1-D signal, ECG. Proposed novel approach for denoising of baseline wander artifact, ensure that the morphological information present in the ECG signal remains preserved and denoising performance is independent of heart rate and external factors. The effectiveness of proposed method is tested on different publically available datasets by comparing with all latest methods. The results prove that proposed method provide far superior denoising results in terms of Minimum Square Error (MSE) and Signal to Noise Ratio (SNR). The effectiveness of the proposed method to preserve morphological information present in the ECG signal is verified in term of the large Correlation Coefficient between original ECG signal and artifact-free ECG signal.
- In the second method, Stationary Wavelet Enhanced Independent Component Analysis with a novel thresholding is used for ocular artifact removal from

EEG. Proposed method incorporates strengths of SWT and ICA. Denoising performance is further improved by using a novel thresholding technique. The proposed denoising method with novel thresholding technique is analyzed in terms of Correlation Coefficient and Mutual Information with other latest methods for different publically available datasets. The superiority of proposed method is also proved by measuring frequency domain Coherence between raw EEG data and artifact-free EEG data.

- To deal with noise and intensity inhomogeneity problem of biomedical images, a new region-based level set model is proposed by integrating concepts of active contour and FCM clustering. In this method, proposed FCM based energy function deal with intensity inhomogeneity of medical image. A spatial function is also used with proposed energy function, which makes this method more advantageous for segmenting noisy images. The proposed method is tested on diverse real medical images, which contain noise as well as intensity inhomogeneity and also on synthetic images. Results show that proposed method has better performance in comparison to other latest methods in term of Segmentation Accuracy of images corrupted by noise. The proposed method has the better segmentation of medical images corrupted by both intensity inhomogeneity as well as noise so proposed method can be utilized for medical applications, where high quality and precise segmentation are required.

6.2 Future Research Scope

Despite the satisfactory performance of proposed methods, some issues are reported and these issues may lead to the future research paradigms. Despite the fact that a modified and faster version of EMD is used in the proposed method for baseline wander removal

from ECG, there is further scope for reduction in the computation time. In this method opening and closing, operations are used as morphological functions. Some more advanced morphological functions [62] may be used to preserve morphological information present in the ECG signal. In the proposed method, a simple artifact analysis algorithm using a wavelet breakdown and identification of ECG components is used to determine the lengths of the complexes and hence the structuring elements. Performance of proposed method highly depend on the dimension of structure elements so some more efficient method for calculating the dimension of structure elements may be used to improve performance.

In proposed method for ocular artifact removal from EEG, bior-4.4 mother wavelet is used in case of Stationary Wavelet Transform. Decomposition is done up to 6^{th} level and the threshold is applied from 3^{rd} to 6^{th} level of decomposition. Performance of proposed method may improve by testing and use various combinations of mother wavelet, level of decomposition and by applying threshold at different levels of decompositions.

The proposed method for biomedical image segmentation is computationally complex since multiple similar convolutions are used repeatedly. As a future work, complexity can be reduced either by using different types of level set methods for implementation of active contours or energy function using different FCM variations [88].

REFERENCES

[1] www.ecglibrary.com

[2] Caton R., "*The electric currents of the brain"*, British Medical Journal, 1995, pp.274-278.

[3] Ivana Despotović, Bart Goossens and Wilfried Philips, "*MRI Segmentation of the Human Brain: Challenges, Methods and Applications*", Computational and Mathematical Methods in Medicine, 2015, Hindawi Publishing Corporation, Article ID 450341.

[4] Anagha S.Kulkarni and R. S. Kamathe, "*MRI Brain Image Segmentation by Edge Detection and Region Selection*", International Journal of Technology and Science, Issue 2, vol.2, 2014.

[5] Shamya C, Shilpa Unnikrishnan M K and Smitha P B," *ECG Denoising Techniques: A Survey*", International Journal of Engineering Research and General Science, Vol 4, Issue 2, March-April, 2016.

[6] S. Thulasi Prasad and S. Varadarajan," *ST Variability Analysis using Triangular Method, Linear Regression and SVM*", International Journal of Scientific & Engineering Research, Vol 6, Issue 10, October-2015.

[7] R.J Croft and R.J Berry, "*Removal of ocular artifact from EEG: a review*", Neurophysiol Clin, Elsevier, 2000, Vol 30, pp: 5-19.

[8] Li. Yanling and Yi. Shen. "*Robust Image Segmentation Algorithm Using Fuzzy Clustering Based on Kernel-Induced Distance Measure*". Proceedings of International Conference on Computer Science and Software Engineering, 2008, Vol-01, pp 1065-1068.

[9] Mahesh S. Chavan, R.A.Agarwala and M.D.Uplane , "*Application of the Chebyshev Type II Digital Filter For Noise Reduction In ECG Signal"* Proceedings of the 5th WSEAS Int. Conf. on Signal Processing, Computational Geometry & Artificial Vision, Malta, September 15-17, 2005 (pp1-8)

[10] Mahesh S. Chavan, R.A.Agarwala and M.D.Uplane, "*Digital Elliptic Filter Application For Noise Reduction In ECG Signal* " , 4th WSEAS International Conference on ELECTRONICS, CONTROL and SIGNAL PROCESSING, Miami, Florida, USA, 17-19 November, 2005 (pp.58-63).

[11] Dr. K. L. Yadav and Sachin Singh, "*Performance evaluation of different adaptive filters for ECG signal processing*", International Journal On Computer Science and Engineering, , 2010,vol. 40, no. 5, pp. 1880-1883.

[12] Muhammad Zia Ur Rahman, Rafi Ahamed Shaik and D.V.RamaKoti Roddy, "*Efficient sign based normalized adaptive filtering techniques for cancelation of artifacts in ECG signals: Application to wireless biotelemetry*", Journal of signal processing, vol. 91, no. 2, pp. 225-239, February 2011.

[13] Ching-Haur Chang ,Kang-Ming Chang and Hsien-Ju Ko, "*Cancellation of high frequency noise in ECG signals using Adaptive filter without external reference*", Proceedings of International Conference on Biomedical Engineering and Informatics, pp. 787—790, Yantai, October 2010.

[14] N. E. Huang, Z. Shen, S. R. Long, M. C. Wu, H. H. Shih, Q. Zheng, N.-C. Yen, C. C. Tung and H. H. Liu, "*The Empirical Mode Decomposition and Hilbert Spectrum for Nonlinear and Nonstationary Time Series Analysis*" Proceedings of the Royal Society London A., 454:903–995, 1998.

[15] Zhi-Dong Zhao, Yu-Quen Chen, " *A new method for Removal of Baseline Wander and Power Line Interference in ECG signals*", Proceedings of the Fifth International Conference on Machine Learning and Cybernetics, Dalian, 13-16 August 2006,pg no. 4342-4347.

[16] A.O Boudraa and J.C Cexus, "*EMD Based signal filtering*", IEEE Transactions on instrumentation and measurement, vol 56,no. 6 , 2007.

[17] Z. Wu and N. E. Huang, "*Ensemble empirical mode decomposition: A noise-assisted data analysis method*," Advances in Adaptive Data Analysis, vol. 1, no. 1, pp. 1–41, 2009.

[18] Na Pan, vai MingI, Mai Peng Un and Pun Sio hang,"*Accurate removal of baseline wander in ECG using EMD*", Proceedings of NFSI & ICFBI, 2007 China,pg no 177-180

[19] Anil Chacko and Samit Ari, "*Denoising of ECG signals using Empirical Mode Decomposition based technique*" IEEE International conference on Advances in Engineering, Science and Management (ICAESM -2012) March 30,31, 2012 pg no 6-9.

[20] L Chmelka and J Kozumpik, "*Wavelet Based Wiener Filter for Electrocardiogram signal denoising*", IEEE, Computers in cardiology, 2005, pp no. 771-774, 2005.

[21] M Kania, M Fereniec, R Maniewski, "*Wavelet Denoising for Multilead High resolution Electrocardiogram(ECG) Signals*", Measurement Science Reiew, Volume 7, Section 2, No.4, pp no. 30-33, 2007.

[22] M Alfaouri and K Daqrouq, " *Electrocardiogram Signal denoising by Wavelet Transform thresholding*", American Journal of Applied Sciences, Vol. 5 Issue 3pp.no 276-281,2008.

[23] N. Li and P.Li, "*An improved algorithm based on EMD-Wavelet for ECG de-noising*", Proceedings of International Joint Conference on Computational Sciences and Optimization, 2009, vol 01, pp: 825-827.

[24] D.T luong, "*Study on the limitations of removal of Baseline noise from electrocardiography signal in measurement using wavelet analysis*", IEEE, ICUFN, 2013.

[25] Z. Wu and N. E. Huang, "*Ensemble empirical mode decomposition: A noise-assisted data analysis method*", Advances in Adaptive Data Analysis, vol. 1, no. 1, pp. 1–41, 2009.

[26] Maria E. Torres, Marcelo A. Colommas, Gaston Schlotthaur and Patrick Flandrin, "*A Complete Ensemble Empirical Mode Decomposition with Adaptive Noise*", IEEE International Conference on Acoust, Speech and Signal Proc. ICASSP-11, pp. 4144-4147, Prague (CZ).

[27] Gurpreet Singh, Gagandeep Kaur and Vineet Kumar, "*ECG Denoising Using Adaptive selection of IMFs through EMD and EEMD* ", ICDSE 2014.

[28] Chee Hung, Henry Chu and Edward J Delp, "*Impulsove noise suppression and background normalization of ECG signals using morphological operators*", IEEE transactions in biomedical engineering, vol 36,no.2,Feb 1989,pg no. 262-273.

[29] Seyfullah Halit OGUZ and Muka Hakan Asyali, " *A morphology based algorithm for baseline wander elimination in ECG records*", International Biomedical Engineering days,1992,pg no. 157-160.

[30] P Sun, Q.H Wu, A.M Weindling, A Finklestein and K Ibrahim, "*An improved morphological approach to background normalization of ECG signals*". IEEE Trnasactions on biomedical engineering, vol 50, No1. January 2003, pg no 117-121.

[31] Zhongguo Liu, Jinliang Wang and Boqiang Liu, "*ECG signal denoising based on morphological filtering*", 5th International conference on Bioinformatics and Biomedical Engineering, 2011.

[32] Manoj Sharma and Hemant Dalal, "*Noise Removal from ECG Signal and Performance Analysis Using Different Filter*", International Journal of Innovative Research in Electronics and Communication (IJIREC), Vol. 1, Issue 2, May 2014, pp 32-39.

[33] Mei-Lin Su and Keh-Shih Chuang, "*An ECG Signal Enhancement Based on Improved EMD*", PIERS Proceedings, Taipei, March 25–28, 2013.

[34] J. Jenitta and A. Rajeswari, "*An Optimized Baseline Wander Removal Algorithm Based on Ensemble Empirical Mode Decomposition*", International Journal of Computer Science, Vol 42, Issue 2, 2015.

[35] Mahipal Singh Choudhry,Akshay Puri and Rajiv Kapoor," *Removal of Baseline Wander from ECG signal using Cascaded Empirical Mode Decomposition and Morphological Functions*" 3rd International Conference on Signal Processing and Integrated Networks (SPIN-2016),Feb 2016.

[36] V. Krishnaveni, S. Jayaraman, S. Aravind, V. Hariharasudhan, and K. Ramadoss, "*Automatic identification and removal of ocular artifacts from EEG using wavelet transform*," Measurement Science Review, vol. 6, section-2, no. 4, pp. 45–57, 2006.

[37] Hong Peng, Bin Hu, Qiuxia Shi, Martyn Ratcliffe, Qinglin Zhao, Yanbing Qi and Guoping Gao, "*Removal of Ocular Artifacts in EEG-An Improved Approach Combining DWT and ANC for Portable Applications*", IEEE Journal of biomedical and health informatics, vol 17,no 3, may 2013.

[38] G. P. Nason and B. W. Silverman, **"***The Stationary Wavelet Transform and some Statistical Applications***",** Wavelets and Statistics, Volume 103 of the series Lecture Notes in Statistics, pp 281-299,Springer Publication,1995.

[39] Shah Aqueel Ahmed, D. Elizabath Rani and Syed Abdul Sattar, "*Detection and Elimination of Ocular Artifacts from EEG Data Using Wavelet Decomposition Technique*", International Journal of Computer Science and Information Security, Vol. 10, No. 1, January 2012.

[40] K.Yasoda and A.Shanmugam, "*Certain analysis on EEG for the detection of EOG artifact using symlet wavelet*", Journal of Theoretical and Applied Information Technology, vol 67, no 01, 2014, pp 54-58

[41] A. Flexer, H. Bauer, J.Pripfl and G. Dorffner, "*Using ICA for removal of ocular artifacts in EEG recorded from blind subjects*", Neural Networks, Science Direct, Elsevier, Vol 18, Issue 7, September 2005, pp 998-1005.

[42] L. Huang, H. Wang and Y. Wang, "*Removal of Ocular Artifact from EEG Using Constrained ICA*", Advanced Engineering Forum, Vols. 2-3, pp. 105-110, 2012.

[43] N. P. Castellanos and V. A. Makarov, "*Recovering EEG brain signals; artefact suppression with wavelet enhanced independent component analysis*," Journal of Neuroscience Methods, vol. 158, 2006.

[44] R. Mahajan and B. I. Morshed, "*Sample entropy enhanced wavelet ICA denoising technique for eye blink artefact removal from scalp EEG dataset*," in Proc. 6th International IEEE/EMBS Conference Neural Eng., 2013, pp. 1394–1397.

[45] M. Mamun, M. Al-Kadi and M. Marufuzzaman, "*Effectiveness of wavelet denoising on electroencephalogram signals*," Journal of Applied Research and Technology, vol. 11, no. 1, pp. 156–160, 2013.

[46] Syarifah Noor Syakiylla, Sayed Daud and Rubita Sudirman, "*Decomposition Level Comparison of Stationary Wavelet Transform Filter for Visual Task Electroencephalogram*", Journal Teknologi, vol 76, Issue 6, 2015.

[47] V. Caselles, F. Catte, T. Coll and F. Dibos, "*A geometric model for active contours in image processing*", Numer. Math., 1993, Vol. 66, No. 1, pp. 1–31.

[48] S. Kichenassamy, A. Kumar, P. Olver, A. Tannenbaum, and A. Yezzi, "*Gradient flows and geometric active contour models*", Proceeding of 5th Int. Conf. Computer Vision, 1995, pp. 810–815.

[49] V. Caselles and R. Kimmel, "*Geodesic Active Contours*", International Journal of Computer Vision, 1997, 22(1), 61–79.

[50] T. Chan and L. Vese, "*Active contours without edges*", IEEE Transactions on Image Processing, 2001, Vol. 10, No. 2, pp. 266–277.

[51] Bing Li and Scott T. Acton, "*Active Contour External Force Using Vector Field Convolution for Image Segmentation*", IEEE Transactions on Image Processing, 2007, vol. 16, no. 8.

[52] Y.Wang and C.He, "*Image segmentation algorithm by piecewise smooth approximation*", EURASIP Journal on Image and Video Processing, 2012, 2012: 16.

[53] Y.Gu, W.Xiong, L.Wang, J.Cheng, W.Huang and J.Zhou, "*A new approach for multiphase piecewise smooth image segmentation*", IEEE International Conference on Image Processing (ICIP), 2014.

[54] M. Airouche, L. Bentabet and M. Zelmat, "*Image Segmentation Using Active Contour Model and Level Set Method Applied to Detect Oil Spills*", Proceedings of the World Congress on Engineering, 2009.

[55] Chunming Li, Chenyang Xu, Changfeng Gui and Martin D. Fox, "*Distance Regularized Level Set Evolution and Its Application to Image Segmentation*", IEEE Transactions on Image Processing, vol 19, no. 12, Dec 2010

[56] B. N. Li, C. Chui, S. Chang and S. H. Ong, "*Integrating spatial fuzzy clustering with level set methods for automated medical image segmentation*", Computers in Biology and Medicine, 2011, vol 41, issue 1, pp: 1–10.

[57] L. Tang, "*A Variational Level Set Model Combined with FCMS for Image Clustering Segmentation*", Mathematical Problems in Engineering, 2014, Article ID 145780.

[58] Wang L, Li C, Sun Q, Xia D and Kao C, "*Active contours driven by local and global intensity fitting energy with application to brain MR image segmentation*", Comput. Med. Imaging Graph. 2009, 33(7):520-531.

[59] Zhang K, Song H and Zhang L, "*Active contours driven by local image fitting energy*", Pattern Recognit. 2010, 43: 1199-1206.

[60] Jili Lu, Mingxing Lin, Qingdong Wang and Yan Huang, "*An Integrated Algorithm of Spatial Fuzzy C-Means Clustering and Level Set for Indoor Scene Image Segmentation*", Journal of Computers, vol. 9, no. 4, April 2014.

[61] Mahipal Singh Choudhry and Rajiv Kapoor, "*Removal of Baseline Wander from ECG using CEEMD and Adaptive Morphogocial Function*", Journal of Chemical and Pharmaceutical Sciences, Issue 4, October 2016.

[62] S.A.Taouli and F.Bereksi-Reguige, "*Noise and baseline wandering suppression of ECG signals by morphological filter*', Journal of Medical Engineering, Vol 34, Issue 02, 2010.

[63] Marıa E. Torres, Marcelo A. Colominas, Gaston Schlotthauer and Patrick Flandrin, "*A COMPLETE ENSEMBLE EMPIRICAL MODE DECOMPOSITION WITH ADAPTIVE NOISE*", IEEE International Conference of Acoustics, Speech and Signal Processing (ICASSP), 2011.

[64] Dewa Gede Hari Wisana , Thomas Sri Widodo , Mochammad Sjabani and Adhi Susanto, "*Identification of ST Segment ECG Signal Using Degestseg Wavelet Detection*", International Journal of Computer Science and Telecommunications, Volume 3, Issue 9, September 2012.

[65] Wang An-donga, Liu Lanb and Wei Qin, "*An Adaptive Morphologic Filter Applied to ECG De-noising and Extraction of R Peak at Real-time*", AASRI Procedia, Elsevier, 2012, Vol 01, pp 474 – 479.

[66] http://physionet.org/physiobank/database/ecgiddb.

[67] http://physionet.nlm.nih.gov/pn3/ ecgiddb.

[68] Mahipal Singh Choudhry and Rajiv Kapoor "*Ocular Artifact Removal from EEG using Stationary Wavelet Enhanced ICA*", International Journal of Control Theory and Applications, 2016, vol: 9, n**o:** 10, pp **:** 4935-4945.

[69] M. Ungureanu, C. Bigan, R. Strungaru and V. Lazarescu, "*Independent Component Analysis Applied in Biomedical Signal Processing*", Measurement Science Review, vol 4, section 2, 2004.

[70] D. B Keith, C. C. Hoge, R. M. Frank, and A. D. Malony, "*Parallel ICA methods for EEG neuroimaging*," 20th International Parallel Distribution Process. Symp., 2006, pp. 25–29.

[71] Ruhi Mahajan and Bashir I. Morshed, "*Unsupervised Eye Blink Artifact Denoising of EEG Data with Modified Multiscale Sample Entropy, Kurtosis and Wavelet-ICA*", IEEE Journal of Biomedical and Health Informatics, vol: 19, Issue: 1, Jan 2015.

[72] Malik M. Naeem Mannan, Myung Y. Jeong and Muhammad A. Kamran, "*Hybrid ICA—Regression: Automatic Identification and Removal of Ocular Artifacts from Electroencephalographic Signals*", Front Hum Neurosci. 2016; 10: 193.

[73] Vandana Roy and Shailja Shukla, "*Automatic Removal of Artifacts from EEG Signal based on Spatially Constrained ICA using Daubechies Wavelet*", International Journal of Modern Education and Computer Science, 2014, vol:7, pp: 31-39

[74] https://physionet.org/mimic2/Signals_Class/eeg.shtml.

[75] Jian-Wu Xu, Hovagim Bakardjian, Andrzej Cichocki and Jose C. Principe, "*A New Nonlinear Similarity Measure for Multichannel Biological Signals*", Proceedings of In-

ternational Joint Conference on Neural Networks, Orlando, Florida, USA, August 12-17, 2007.

[76] Umberto Melia, Marc Guaita, Montserrat Vallverdú, Cristina Embid, Isabel Vilaseca, Manel Salamero and Joan Santamaria, "*Mutual information measures applied to EEG signals for sleepiness characterization*", Medical Engineering and Physics, Elsevier, 2015, vol: 37, Issue:3, pp: 297–308.

[77] Mahipal Singh Choudhry and Rajiv Kapoor, "*A Novel Fuzzy Energy Based Level Set Method for Medical Image Segmentation*", Cogent Engineering, Taylor & Francis, 2018.

[78] S. Chen and D. Zhang, "*Robust Image Segmentation Using FCM with Spatial Constraints Based on New Kernel-Induced Distance Measure*", IEEE Transaction on System, man and Cybernetics-Part b: Cybernetics, 2004, vol. 34, no. 4.

[79] Mumford and J. Shah, "*Optimal Approximations by Piecewise Smooth Functions and Associated Variational Problems*"**,** Communications on Pure and Applied Mathematics, 1989, vol. XLII, pp: 577-685.

[80] C.Li, R. Huang, Z. Ding, J. C. Gatenby, D. N. Metaxas and John C. Gore, "*A Level Set Method for Image Segmentation in the Presence of Intensity Inhomogeneities with Application to MRI*", *IEEE Transactions on Image Processing,* 2011, vol. 20, no. 7.

[81] T. Chan and L. Vese, "*Active contours without edges*", *IEEE Transactions on Image Processing*, 2001, vol. 10, no. 2, pp. 266–277.

[82] L.A. Vese and T. F. Chan, "*A Multiphase Level Framework for Image Segmentation using Mumford and Shah Model*", International Journal of Computer Vision, 2002, Vol: 50, Issue: 2, pp: 271-293.

[83] Cunliang Liu, Yongguo Zheng, Zhenkuan Pan and Guodong Wang, "*A Fast Algorithm for Multiphase Image Segmentation: The Split-Bregman-Projection Algorithm*", International Journal of Modeling and Optimization, Vol. 2, No. 1, February 2012.

[84] N.Rajesh Kumar and J.Uday Kumar, "*A Spatial Mean and Median Filter for Noise Removal in Digital Images*", International Journal of Advanced Research in Electrical, Electronics and Instrumentation Engineering, 2015, vol. 4, Issue 1.

[85] https://openfmri.org/dataset/

[86] adni.loni.usc.edu/methods/mri-analysis/adni-standardized-data/

[87] Jayaram K. Udupa , Vicki R. LaBlanc , Hilary Schmidt , Celina Imielinska and Punam K. Sahaa , "*A Methodology for Evaluating Image Segmentation Algorithms*" Computerized Medical Imaging and Graphics, 2006, vol: 30, pp: 75–87.

[88] Mahipal Singh Choudhry and Rajiv Kapoor, "*Performance Analysis of Fuzzy C-Means Clustering Methods for MRI Image Segmentation*", Procedia Computer Science, Elsevier, vol: 89, pp: 749 – 758.

[89] Maryam Rastgarpour and Jamshid Shanbehzadeh, "*A New Kernel-Based Fuzzy Level Set Method for Automated Segmentation of Medical Images in the Presence of Intensity Inhomogeneity*", Computational and Mathematical Methods in Medicine, Hindawi Publishing Corporation, Volume 2014, Article ID 978373.

AUTHOR BIOGRAPHY

Mahipal Singh Choudhry,

Associate Professor,
Department of Electronics & Communication Engineering,
Delhi Technological University, Delhi, India
Email: **msc_1976@yahoo.com**

Mahipal Singh Choudhry received the Bachelor of Engineering (B.E) and Master of Engineering (M.E) from Malviya Regional Engineering College (Now Malviya National Institute of Technology), Jaipur, Rajasthan, India, in the year 1998 and 2001 respectively. Presently, he is working as Associate Professor, in the Department of Electronics & Communication Engineering, Delhi Technological University, Delhi, India-110042. His research interests include Biomedical Signal Analysis, Biomedical Image Analysis, Digital Signal and Image Processing.